Environmental Science & Technology

Article

pubs.acs.org/est

Emission and Atmospheric Transport of Particulate PAHs in Northeast Asia

Yayoi Inomata,[*,†] Mizuo Kajino,[‡,§] Keiichi Sato,[†] Toshimasa Ohara,[∥] Jun-Ichi Kurokawa,[∥,†] Hiromasa Ueda,[⊥] Ning Tang,[#,$] Kazuichi Hayakawa,[#] Tsuyoshi Ohizumi,[†] and Hajime Akimoto[†]

[†]Asia Center for Air Pollution Research, 1182, Sowa, Nishi-ku, Niigatashi, Niigata, 950-2144, Japan

[‡]Meteorological Research Institute, 1-1, Nagamine, Tsukuba, Ibaraki, 305-0052, Japan

[§]Pacific Northwest National Laboratory, P.O. Box 999, Richland, 99352 Washington, USA

[∥]National Institute for Environmental Studies, 16-2, Onogawa, Tsukuba, Ibaraki, 305-8506, Japan

[⊥]Toyohashi University of Technology, Toyohashi, Aichi, 441-8580, Japan

[#]Graduate School of Natural Science and Technology, Kanazawa University, Kakuma-machi, Kanazawa, 920-1154, Japan

[$]Hyogo College of Medicine, 1-1, Mucogawacho, Nishinomiya, Hyogo, 663-8501, Japan

Supporting Information

ABSTRACT: The emission, concentration levels, and transboundary transport of particulate polycyclic aromatic hydrocarbons (PAHs) in Northeast Asia were investigated using particulate PAH measurements, the newly developed emission inventory (Regional Emission inventory in ASia for Persistent Organic Pollutants version, REAS-POP), and the chemical transport model (Regional Air Quality Model ver2 for POPs version, RAQM2-POP). The simulated concentrations of the nine particulate PAHs agreed well with the measured concentrations, and the results firmly established the efficacy of REAS/RAQM2-POP. It was found that the PAH concentrations in Beijing (China, source region), which were emitted predominantly from domestic coal, domestic biofuel, and other transformations of coal (including coke production), were approximately 2 orders of magnitude greater than those monitored at Noto (Japan, leeward region). In Noto, the PAH concentrations showed seasonal variations; the PAH concentrations were high from winter to spring due to contributions from domestic coal, domestic biofuel, and other transformations of coal, and low in summer. In summer, these contribution were decrease, instead, other sources, such as the on-road mobile source, were relatively increased compared with those in winter. These seasonal variations were due to seasonal variations in emissions from China, as well as transboundary transport across the Asian continent associated with meteorological conditions.

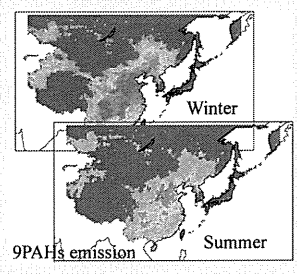

1. INTRODUCTION

Polycyclic aromatic hydrocarbons (PAHs) are highly carcinogenic to humans.[1] In general, PAHs are emitted from domestic, industrial, power plant, traffic, and open biomass burning sources during the incomplete combustion and pyrolysis of fossil fuels and biomass and during coke production.[2−4] China is one of the largest PAH-emitting countries in the world, and the high emission is associated with rapid economic and industrial growth.[3] High concentrations of PAHs were observed in Chinese urban sites.[5−7] Furthermore, comparatively high PAH concentrations have been observed at other locations in East Russia, South Korea, and Japan, which are related to the transboundary transport of PAHs from China.[5−7] PAHs originating from China have received increased attention as a potential human health risk in Northeast Asia.[8]

Although many measurements of particulate PAHs have been conducted,[5−7] these studies are insufficient to elucidate the pollution by PAHs in Northeast Asia. According to the European Monitoring and Evaluation Program (EMEP) project, which operates under the convention of long-range transboundary air pollution, transboundary transport and its contribution to the total deposition of PAHs is a significant source of POP pollution in Europe.[9] To evaluate the pollution levels and transboundary transport of PAHs in Northeast Asia, it is necessary to investigate the temporal and spatial variations of PAHs using a chemical transport model and a monitoring approach.

An inventory of PAH emissions is required to simulate PAH concentrations in the atmosphere. Until now, PAH emission inventories have been reported for several countries, such as the former Union of Soviet Socialist Republics, the European EMEP countries, the United States, and the United Kingdom.[10−13] In Asia, a few PAH emission inventories have been reported; Zhang and Tao reported the global inventory on a country basis.[3] The PAH emission inventory reported by Xu et al. and Zhang et al. focused on China only.[2,14] There is no available grid-based PAH emission inventory in Northeast Asia. Although the outflow of PAHs from China has been reported with the use of China's emission inventory,[15−17] a comprehensive view has not yet been obtained.

Received: October 20, 2011
Revised: March 19, 2012
Accepted: March 22, 2012
Published: March 22, 2012

To investigate the transboundary transport of particulate PAHs in Northeast Asia, measurements have been taken at several monitoring stations by a PAH-monitoring network in Northeast Asia that was established by a group at Kanazawa University under several projects, one of which is the "Study on potential threat caused by organic pollutants in the Japan Sea region".[5−7] In the present study, the spatial and temporal distributions of particulate PAH concentrations were investigated using our newly developed PAH emission inventory for Northeast Asia, applying the Regional Emission inventory in ASia (REAS) for Persistent Organic Pollutants version (REAS-POP),[18] and the Regional Air Quality Model ver2 for Persistent Organic Pollutants (RAQM2-POP) we developed.[19] The REAS/RAQM2-POP was verified by comparing the measured and simulated particulate concentrations for 9 PAHs (Flu, Pyr, BaA, Chr, BbF, BkF, BaP, IcdP, and BghiP) at the Beijing (China, source region) and Noto (Japan, approximately several thousand kilometers leeward from the eastern coast of China) monitoring sites.

2. MATERIALS AND METHODS

2.1. Emission Inventory. We developed the first gridded emission inventory of PAHs, the Regional Emission inventory in ASia for Persistent Organic Pollutants version (REAS-POP), in Northeast Asia. This method of estimating emissions is shown in Figure S1 in the Supporting Information (SI). The REAS-POP includes emission data for 16 PAHs (2 rings: naphthalene (NaP); 3 rings: acenaphthylene (Acy), acenapthene (Ace), fluorene (Flo), phenanthrene (Phe), and anthracene (Ant); 4 rings: fluoranthene (Flu), pyrene (Pyr), benz[*a*]anthracene (BaA), and chrysene (Chr); 5 rings: benzo[*b*]fluoranthene (BbF), benzo[*k*]fluoranthene (BkF), benzo[*a*]pyrene (BaP), and dibenz[*a,h*]anthracene (DahA) and 6 rings: indeno[1,2,3-*cd*]pyrene (IcdP) and benzo[*g,h,i*]perylene (BghiP)) that are listed as priority pollutants by the United States Environmental Protection Agency (USEPA).[20] The available measurement data used to validate REAS-POP was limited to 9 PAHs (Flu, Pyr, BaA, Chr, BbF, BkF, BaP, IcdP, and BghiP) because volatile PAHs that contain 2 or 3 rings could not be recovered by collecting airborne particulates. Therefore, the emission inventory in this study was focused on these 9 PAHs.

The monthly emission of each PAH species was estimated by following equation.

$$E_{(i)} = FC_d \times EF_{(i)} \times MF + FC_{nd}/12 \times EF_{(i)} + TR/12 \times EF_{(i)} + E_{BC} \times EF_{(i)/BC}$$

where

E is the each PAH emission (mg mon^{-1});
(i) is the PAH species;
FC_d is the fuel consumption rate for the domestic sector by REAS (mg yr^{-1});[18]
EF is the emission factor of each PAH (mg kg^{-1} or mg km^{-1});
MF is the grid-based monthly factor;[21,22]
FC_{nd} is the fuel consumption rate for sectors other than the domestic one by REAS (mg yr^{-1});[18]
TR is the traffic fuel consumption rate for on-road mobile sources by REAS (km yr^{-1});[18]
E_{BC} is the monthly black carbon (BC) emission of open biomass burning (mg mon^{-1}) from the Global Fire Emissions Database version 3 (GFEDv3);[23]
$EF_{(i)/BC}$ is the ratio of each PAH emission (mg) against BC emission (mg) by open biomass burning.

The PAH emissions are gridded at 0.5° × 0.5°, and these were interpolated into the model grids with a 60 × 60 km resolution. The period is from 2000 to 2005.

We describe the details of fuel and traffic fuel consumption rates by REAS, the emission factors, and the emission from open biomass burning in the following sections.

2.1.1. Annual Fuel Consumption Rates by REAS and Monthly Factors. Fuel consumption rates were derived from the Regional Emission inventory in ASia (REAS).[18] The fuel consumption rate was estimated at the province and country levels and was divided into a 0.5° × 0.5° grid by using several databases, including population data, information on the positions of large point sources, a land cover data set, and a land area data set.[18]

The fuel consumption rates were classified into two sources, stationary and on-road mobile sources. The fuel consumption rates of the stationary sources were classified into the following five economic sectors: domestic, industry, other transformation, power plant, and others. The fuel consumption rates of these stationary sources were also categorized by the following seven fuel types: coal (hard coal, brown coal, and derived coal (coke oven)), gas (natural gas), light fuel (motor gasoline and kerosene), diesel oil, heavy fuel (heavy fuel oil and crude oil), biofuel (fuel wood, crop residue, and animal waste), and others (municipal waste and charcoal). It is noted that coke and aluminum production, which are considered to be the sources of PAHs, are classified into "other transformation of coal" and "coal industry", respectively. Furthermore, the traffic fuel consumption rates of the on-road mobile sources were classified into seven types (light-duty gasoline vehicles, heavy-duty gasoline vehicles, light-duty diesel vehicles, heavy-duty diesel vehicles, gasoline buses, diesel buses, and motorcycles).

These fuel consumption rates were based on the annual average value. To estimate the monthly fuel consumption rate, usage of the space-heating component of residential energy was divided into monthly values because the space-heating component of residential energy use depends on the outdoor temperature. The MF was estimated using the ratio of monthly usage of the space-heating component of residential energy to the annual one.[21,22]

2.1.2. PAH Emission Factors. The factors affecting the emission of gas and particulate PAHs in Northeast Asia were collected from the literature (SI Table S1, S2, S3).[2,12,14,20−43] It was reported that emission factors varied widely depending on the combustion conditions (e.g., temperature, water content, and fuel type).[34] In addition, the data for emission factors for each source in this study was very limited; the number of emission factors for each source was in the range of 1−25. Therefore, the adopted emission factors included great uncertainty. We have attempted to perform sensitivity calculations using the maximum, minimum, and median values of the emission factors (see Section 3.3). The median values of emission factors were adopted in this study. If there were no available data for Northeast Asia on the emission factors of any of the sources, typical values from other parts of the world were adopted.[12] For the sources that had no information regarding the emission factors, the emission factors were considered to be 0.

2.1.3. PAH Emission from Open Biomass Burning by GFEDv3. PAH emission from open biomass burning was estimated using the burned area, the BC emission rate, and the

PAH and BC emission factors. The burned area and the BC emission rate were derived from GFEDv3, with a spatial resolution of 0.5° × 0.5° latitude/longitude and a monthly time resolution.[23] The burned area was classified into two types according to the land use categories in GFEDv3, agricultural waste burning and forest fire-type burning, based on the United States Geological Survey (USGS) land use data. The BC emission factor from open biomass burning was set to the median value (0.66 g kg^{-1}) of the available data set.[44−46] The emission factor of PAHs from BC emission was also determined to be the median value of the data set (SI Table S4).[34,40]

2.2. Off-line Coupled Meteorology (WRF)-Chemical Transport Model (RAQM2-POP). The Regional Air Quality Model ver2 for Persistent Organic Pollutants (RAQM2-POP)[19], aerosol chemical transport model, was used to simulate the PAHs. This model was used to investigate the long-range transport and deposition of sulfate, nitrate, and dust particles over Northeast Asia.[48−50] We developed RAQM2 to simulate the emission, long-range transport, and dry/wet deposition in particulate and gaseous phase PAHs. In RAQM2-POP, several processes such as advection, turbulent diffusion, aerosol dynamics (nucleation, condensation/evaporation, coagulation), partitioning between the gaseous and particulate phase, dry/wet deposition in particulate and gaseous phase, and degradation in the atmosphere were considered (SI Table S5). These specific parameters were almost the same as those used in the Meteorological Synthesizing Center-East (MSCE)-POP model, developed by MSC-E for the European Monitoring and Evaluation Programme (EMEP) region,[51] except aerosol dynamics and cloud microphysical processes. The PAH boundary condition was set to 0, because China is considered to be the dominant emission country. The specifics of RAQM2-POP have been described by Kajino et al.[19]

The Weather Research and Forecasting model version 3.0 (WRF) was used to provide the meteorological field for RAQM2-POP.[52] The National Centers for Environmental Prediction (NCEP) final operational analysis data (FNL), ds083.2 (http://dss.ucar.edu/data sets/ds083.2), were used to provide the initial and boundary conditions for WRF (http://dss.ucar.edu). The WRF and RAQM2-POP model domains cover most areas of the Northeast Asian countries. The horizontal grid resolution is 60 km with a Lambert conformal map projection, and there are 27 vertical layers from the ground surface to 100 hPa for WRF and 12 layers from the ground to 10 km (at approximately 50, 150, 300, 500, 750, 1500, 2500, 3500, 4500, 6000, 7500, and 8950 m) for RAQM2-POP. Emissions, concentrations, wet depositions, and dry depositions were output on an hourly basis.

2.3. Aerosol Observation and Chemical Analysis. The measurement of particulate PAH concentrations was conducted at two monitoring sites in Beijing (China, Longitude 116.4°E, Latitude 40.0°N) and Noto (coastal site on the Sea of Japan in Japan, Longitude 136.9°E, Latitude 37.5°N). These concentrations were used to validate the REAS/RAQM2-POP. Under prevailing westerly winds over midlatitudes, Beijing is considered to be the source monitoring site, and Noto is considered to be the leeward monitoring site.

At the Beijing monitoring site, sampling was conducted on the rooftop of a three-story building at the Chinese Academy of Sciences, Center for Ecological Research, which is located in Chaoyang District, during the period from 8 March 2005 to 13 April 2005 and from 10 May 2005 to 26 May 2005 at 1-day intervals. The Noto monitoring site is located on the Japanese main island (2.1 km downwind from the coastal line) in the Noto peninsula on the coast of the Sea of Japan. Airborne particulate matter was collected continuously from 31 December 2004 to 28 December 2005 at 1-week intervals. There were no major PAH emission sources around the Noto monitoring site. At both sites, the airborne particulate matter was collected on quartz-fiber filters (2500QAT-UP, Pallflex Products, Putnam, CT) using high-volume air samplers (Beijing, HV-1000F, Shibata, Japan; Noto, AH-600, Shibata, Japan).

Nine particulate PAHs (Flu, Pyr, BaA, Chr, BaP, BbF, BkF, BghiP, IcdP) were analyzed by HPLC with fluorescence detection at Kanazawa University. The details of the sampling and analysis have been described previously.[6,53]

3. RESULTS AND DISCUSSION

3.1. Emission of 9 PAHs in Northeast Asia. Figure 1 shows the geographical distribution of the annual emissions of the 9 PAHs at a resolution of 0.5° × 0.5° in Northeast Asia in 2005 (RAQM2-simulated domain; longitude 84−161°E, latitude 16−55.5°N). China was shown to be the most significant contributor of the 9 PAH contaminants in Northeast Asia. In particular, elevated levels of the 9 PAHs were noted in the North China Plain, the East coast of China, Guizhou, Sichuan Basin, and Northeastern China. The estimated annual emission of the 9 PAHs in China in 2005 was approximately 9.6 Gg yr^{-1} (1.3 mg m^{-2} $year^{-1}$), which accounted for 92% of the total emissions (10.5 Gg yr^{-1}) in Northeast Asia in 2005. According to a previous report,[2] the total emission of the 9 PAHs in China in 2003 was estimated to be 7.1 Gg yr^{-1}. This estimation was close to ours (8.0 Gg yr^{-1}) for 2003. The emission from the eastern part of Russia (East Russia) was estimated to be 0.19 Gg yr^{-1} (0.13 mg m^{-2} $year^{-1}$, 1.8% of the total emission of the 9 PAHs in Northeast Asia); North Korea, 0.29 Gg yr^{-1} (1.7 mg m^{-2} $year^{-1}$, 2.7%); Mongolia, 0.021 Gg yr^{-1} (0.014 mg m^{-2} $year^{-1}$, 0.20%); Japan, 0.020 Gg yr^{-1} (0.029 mg m^{-2} $year^{-1}$, 0.19%); South Korea, 0.020 Gg yr^{-1} (0.13 mg m^{-2} $year^{-1}$, 0.29%); and Taiwan, 0.0028 Gg yr^{-1} (0.045 mg m^{-2} $year^{-1}$, 0.0036%).

The estimated emissions and percentages of each species to the total emission of the 9 PAHs in 2005 were as follows: 2.2 Gg yr^{-1} (21%) for Flu, 1.9 Gg yr^{-1} (18%) for Pyr, 0.90 Gg yr^{-1} (9%) for BaA, 0.93 Gg yr^{-1} (9%) for Chr, 1.4 Gg yr^{-1} (13%) for BaP, 1.4 Gg yr^{-1} (13%) for BbF, 0.52 Gg yr^{-1} (5%) for BkF, 0.59 Gg yr^{-1} (6%) for BghiP, and 0.75 Gg yr^{-1} (7%) for IcdP. The largest emission was that of Flu, which contains 4 benzene rings, followed by that of Pyr (4 rings), BbF (5 rings), and that of BaP (5 rings) (see SI Figure S2). The emission profiles reflect the emission patterns from China, which is the dominant PAH-emitting country in Northeast Asia. However, the emission sources of the 9 PAHs vary considerably from county to country. In China, the dominant PAH sources were domestic coal (47%), domestic biofuel (18%), and other coal transformations, including coke production (29%). Xu et al. also estimated that domestic biofuel, domestic coal, and coke production were the dominant sources of PAH emission in China in 2003.[2] Open biomass burning contributes 0.3% of China's emissions. In East Russia, North Korea, and Mongolia, domestic biofuel (4% for East Russia, 33% for North Korea, and 43% for Mongolia), domestic coal (28% for East Russia, 61% for North Korea, and 11% for Mongolia), and other coal transformations (37% for East Russia, 3% North Korea, and 4% for Mongolia) were also dominant sources. Furthermore, the emission from open biomass burning was also a large contributor in East Russia (31%) and Mongolia (38%).

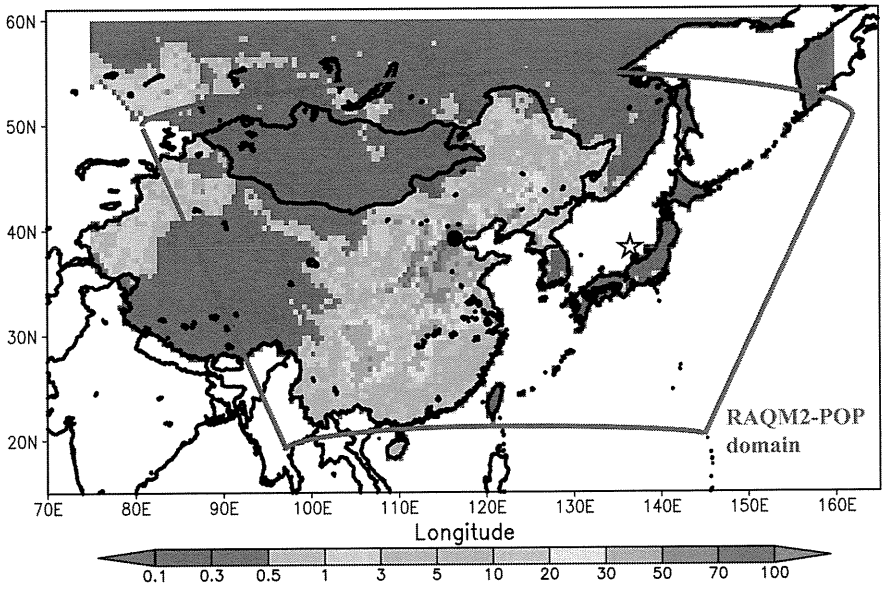

Figure 1. Spatial distributions of the annual emissions of 9 PAHs at a 0.5° × 0.5° resolution in 2005 in Northeast Asia by REAS-POP. The scale is in the units of mg yr^{-1} m^{-2}. ● indicates the location of Beijing, and ☆ indicates the location of Noto. The model domain used by RAQM2-POP is also shown.

In Japan and Taiwan, the major emission source was on-road mobile, accounting for 68% and 44% of the PAH emissions, respectively. These results are consistent with the results of the cluster analysis and factor analysis, which were based on the measurement data and demonstrated that the main source of PAHs in Japanese cities (Kanazawa, Tokyo, and Sapporo) was automobiles, especially diesel-engine vehicles.[5] The South Korean emissions originated primarily from on-road mobile sources (35%), industry (32%), other coal transformations (15%), and domestic coal (11%).

These PAH emissions, in this case BaP, show clear seasonal variation with high levels in winter to spring and low levels in summer (SI Figure S3a). The seasonal variation can be attributed to domestic coal and domestic biofuel sources because of the use of heating systems. Conversely, the relative contribution of the other coal transformations increased in summer (SI Figure S3b).

3.2. Evaluation of PAH Pollution in Northeast Asia.

3.2.1. Seasonal Variation of the Measured and Simulated PAH Concentrations at the Beijing and Noto Monitoring Sites. Figure 2 shows the comparison between the measured and simulated particulate PAH concentrations at the Beijing and Noto monitoring sites. At both sites, the simulated PAH concentrations generally agreed well with the measured concentrations. It was noted that the PAH concentrations measured in Beijing were 2 orders of magnitude greater than those measured in Noto.

At the Beijing monitoring site, the observed (simulated) average concentrations and the standard deviation of 6 PAHs were as follows: 6510 ± 6540 (7480 ± 5790) pg m^{-3} for Pyr, 6520 ± 5810 (5800 ± 3330) pg m^{-3} for Chr, 8100 ± 5890 (10100 ± 6940) pg m^{-3} for BbF, 3050 ± 2280 (2550 ± 1440) pg m^{-3} for BkF, 5790 ± 5060 (9250 ± 4350) pg m^{-3} for BaP, and 4250 ± 3070 (4440 ± 2210) pg m^{-3} for IcdP. The correlation coefficient for each species ranged from 0.30 to 0.58 (SI, Table S6). Pyr exhibits the highest concentration, which contains 4 benzene rings. The concentrations of PAHs gradually decreased from March to May. Additionally, the PAH concentrations in Beijing were characterized by daily variations. It is also noteworthy that the simulated PAH concentrations were significantly underestimated when measured concentrations were very high (15–16 March 2005 and 6 April 2005). Relatively higher concentrations were observed under weak wind speeds (data not shown), which causes weak dispersion of PAH concentrations in air. Furthermore, emission would also contribute to this discrepancy. In the RAQM2-POP, the emission was given as the monthly average value, and simulated concentrations were the average values on the grid (resolution 60 × 60 km), which cannot identify local sources on a daily basis. The large discrepancy between measurements and simulation would result from the contribution of the local source.

At the Noto monitoring site, the observed (simulated) average concentrations and standard deviations for the particulate 9 PAHs were as follows; 87.6 ± 77.2 (14.5 ± 21.9) pg m^{-3} for Flu, 60.8 ± 55.0 (11.5 ± 14.1) pg m^{-3} for Pyr, 14.1 ± 11.8 (47.8 ± 43.2) pg m^{-3} for BaA, 34.5 ± 26.3 (38.8 ± 35.3) pg m^{-3} for Chr, 44.9 ± 36.6 (34.3 ± 44.6) pg m^{-3} for BbF, 16.5 ± 12.2 (4.6 ± 5.7) pg m^{-3} for BkF, 23.5 ± 16.4 (13.1 ± 14.7) pg m^{-3} for BaP, 27.6 ± 17.6 (19.0 ± 16.2) pg m^{-3} for BghiP, and 21.3 ± 15.5 (4.74 ± 6.09) pg m^{-3} for IcdP (SI, Table S7). Although several simulated species, including Flu, Pyr, BkF, and IcdP, were underestimated, the seasonal variation (high in winter to spring and low in summer) is well reproduced by the simulation. The underestimation of several PAHs might be caused by the values set for several parameters such as degradation, dry/wet deposition during the long-range transport, and gas-particle partitioning. These parameters are subjects of future investigation. Compared with the source region (Beijing), the correlation coefficient of each PAH species between the measured and simulation values at Noto was high (0.73–0.87). One reason for this is that the measured concentrations at Beijing were strongly influenced by the emission from the local source. The large variation in concentrations was reduced due to the longer sampling time (1 week) at Noto. Furthermore, the higher correlation suggests that the variations in concentrations at remote sites such as Noto are mainly controlled by synoptic scale disturbances

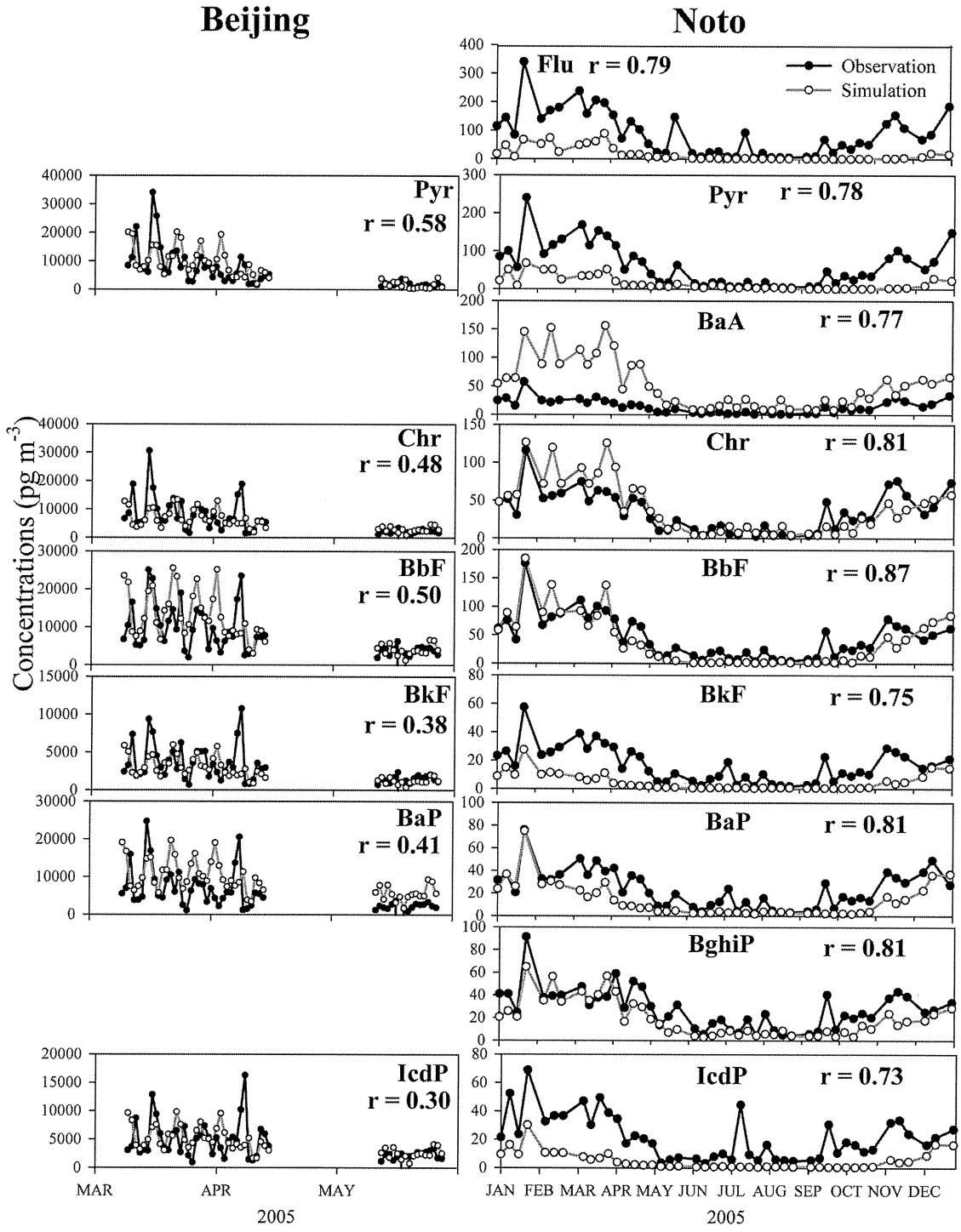

Figure 2. Comparison of the measured and simulated concentrations of the particulate 9 PAHs at Beijing (left panel) and Noto (right panel). The data at Beijing were a one-day average from March to May in 2005, whereas the Noto data were a weekly average from January to December in 2005. *r* is the correlation coefficient between the measured and simulated particulate concentrations.

(fronts, cyclones, and anticyclones), which are generally well predicted by regional-scale models.

These results also suggest that our newly developed REAS/RAQM2-POP is reasonably accurate in simulating the atmospheric particulate concentrations of 9 PAHs.

3.2.2. Spatial and Seasonal Variations in BaP Concentrations in Northeast Asia. Figure 3 shows the simulated temporal variation of BaP concentrations at the Noto monitoring site with these dominant sources. As shown in Figure 2, BaP concentrations showed clear seasonal variation with higher values in winter to spring and lower values in summer. The dominant source of BaP at Noto was domestic biofuel (11–18%), domestic coal (20–59%), and other transformation of coal (4–18%) from winter to spring. The contribution from domestic biofuel and coal combustion decreased toward summer, while the contribution from other sources was relatively increased. In particular, the contribution from the on-road mobile source was relatively higher in summer (10–17%).

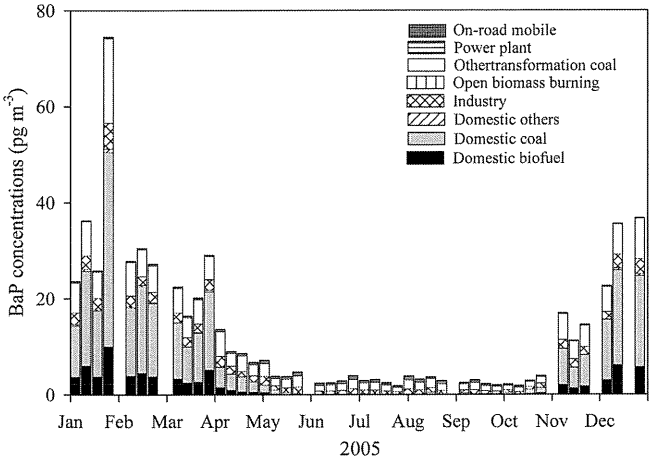

Figure 3. Temporal variation of simulated BaP concentrations at the Noto monitoring site with these source profiles.

Figure 4 shows the horizontal distributions of the simulated seasonal averaged particulate BaP concentrations and wind vectors near the surface. BaP was selected as a representative for the characterization of the total 9 PAHs because its high toxicity causes a greater health impact. In winter (Figure 4a), high BaP concentrations were observed over a wide region in China, and we observed the transboundary transport of BaP from the Asian continent toward the Japanese islands. Northwesterly or westerly winds prevailed over Northeast Asia during the observation period, which suggests that BaP is long-range transported from Northeast Asia to the Japanese islands. In spring (Figure 4b), the concentrations of BaP at the Noto monitoring site were decreased compared with those in winter under the weak westerly wind, suggesting that the transboundary transport was weakened. In contrast, as shown in Figure 4c, southerly and southwesterly winds prevailed over the Pacific Ocean under the Pacific High pressure system, which blocks transboundary transport of BaP from the Asian continent. In autumn (Figure 4d), the transition season from summer to winter, the transboundary transport of BaP is reinforced again.

These results suggest that the seasonal variation of BaP emission and the prevailing meteorological conditions strongly controlled transboundary transport in Northeast Asia. Under westerly winds, domestic coal, domestic biofuel, and other coal transformations, including coke production in China, were the dominant BaP sources at the Noto station, based on the source profile.

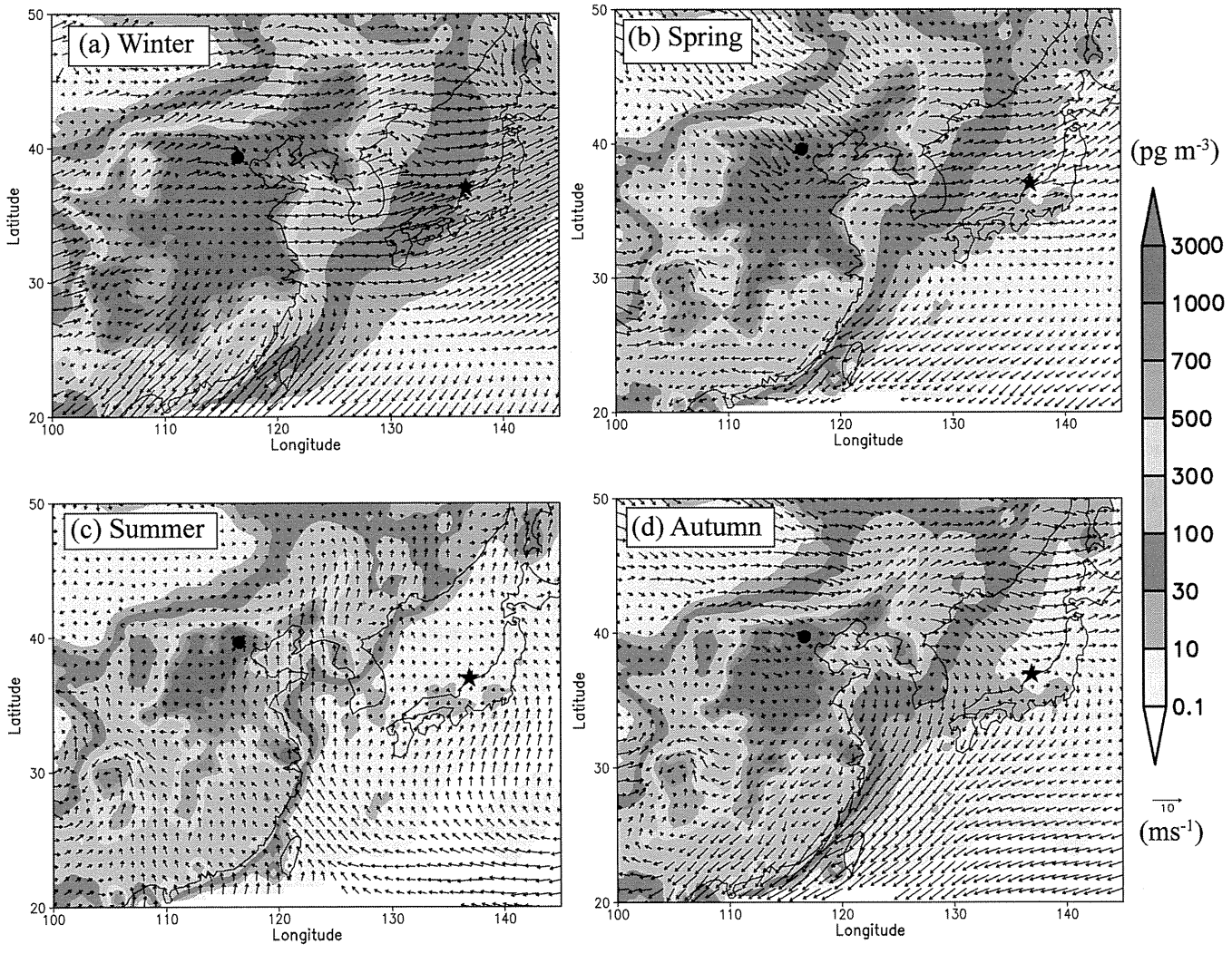

Figure 4. Spatial distributions of seasonal averaged BaP concentrations (a) Winter (December, January, and February), (b) Spring (March, April, May), (c) Summer (June, July, and August), and (d) Autumn (September, October, and November). The color scale is in units of pg m^{-3}. ● indicates the location of Beijing monitoring site, and ★ indicates the location of Noto monitoring site.

When westerly winds are weak in summer, relative contributions from other sources such as on-road mobile source were increased. The seasonal variation and the source profiles of the other PAH species were similar to those of BaP.

3.3. Uncertainty in Emission Factors for Emission Estimates. The majority of the emission factors that were used in this study were derived from the data from China. We have no specific emission factors for other Asian countries, with the exception of the on-road mobile sources in Japan and several data from Taiwan. In addition, the reported emission factors displayed large variations depending on the combustion processes, fuel composition, and oxygen supply. It is also expected that the emission factors of each category change rapidly as a result of technological innovations that have occurred over several decades, for instance, the elimination of dust. To set adequate emission factors, we conducted sensitivity calculations by changing the emission factors.

At first, the emission factor for each source was set to the same value, 1, for all of the Northeast Asian countries. Under this assumption, the seasonal variation (high in the winter and low in the summer) that was observed at Noto could not be simulated. In addition, the simulated concentrations in the summer at Noto were higher than those in the winter and spring. According to the trajectory analysis calculated for several years, most air masses arriving at Noto in summer were transported from the south or southwestern part of the Japanese islands.[54] The results of the sensitivity calculations with the high concentrations of the 9 PAHs in the summer at Noto suggest that the PAH emissions from the Japanese islands are too large. These results also imply that the same emission factor should not be used for all of the Northeast Asian countries. In fact, Wang et al. reported that the emission factors of 16 PAHs from on-road mobile sources in China were 100 times higher than those in Europe and the United States.[35] In this study, the emission factors of 9 PAHs that were derived from on-road mobile sources in China were approximately 100−1000 times greater than those in Japan.[36,39] Based on these data, the emission factor of each source (with the exception of the on-road mobile sources) in the developed countries was set at $^1/_{100}$ of those in the developing countries in this study. Based on the country's Gross Domestic Product (GDP) per capita,[55] we arbitrarily divided the countries in Northeast Asia into two groups: developing countries (China, East Russia, Mongolia, and North Korea) and developed countries (Japan, South Korea, and Taiwan). As a result, the seasonal variation of the particulate PAH concentrations at Noto could be simulated well.

Second, we conducted sensitivity calculations by changing the emission factors of the domestic biofuel and domestic coal sources, which are the dominant contributors of particulate PAH emissions (SI Table S8). The range of BaP emission factors used in the data set varied from n.d. (not detected) to 88.8 mg kg^{-1} for domestic coal and 0.04−6.6 mg kg^{-1} for domestic biofuel.[2,20,26,27,42] For the emission factors of the other coal transformations source, which are also recognized as major PAH sources, we could not conduct the sensitivity calculations because there was only one source of data. Figure 5 shows the results of the sensitivity calculations for BaP at Noto using different emission factors (the maximum, median, and minimum values of the emission factors data set). The simulaed concentrations using the median value of emission factors were reasonably consistent with the observed concentrations. Conversely, the concentrations simulated by using the maximum emission factor were approximately 100 times higher than the observed concentrations. In addition, it appears that the simulated concentrations were less than approximately $^1/_{10}$ of the measured concentrations when the minimum emission factor was used. It was reported that the emission factors of PAHs from coal combustion vary greatly depending on combustion conditions (temperature and oxygen supply associated with type of combustor), combustion efficiency, and component of coal.[41] Regarding domestic biofuel combustion, the emission factors varied by several orders of magnitude due to many factors, including fuel moisture, combustion temperature, oxygen supply, and combustion place.[40] In fact, PAHs would be emitted under various combustion conditions and different fuel compositions. Because the results using the sensitivity calculations showed that the median value of emission factor predicted the observed BaP concentration well, we adopted the median value of the data set as the emission factor for each category.

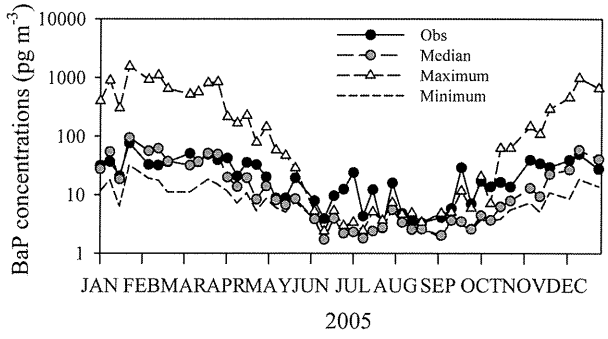

Figure 5. Sensitivity calculation for the simulated BaP concentrations at the Noto monitoring site using different emission factors. In the data set of emission factors for the domestic coal and domestic biofuel sources, the maximum, minimum, and median values were used for the sensitivity calculations.

■ ASSOCIATED CONTENT

Ⓢ Supporting Information

Additional material as noted in the text. This material is available free of charge via the Internet at http://pubs.acs.org.

■ AUTHOR INFORMATION

Corresponding Author

*Phone: +81-25-263-0558; fax: +81-25-263-0567; e-mail: inomata@acap.asia.

Notes

The authors declare no competing financial interest.

■ ACKNOWLEDGMENTS

This research was financially supported by the Environment Research and Technology Development Fund (Project No. B-0905 and A-1101) of the Ministry of the Environment, Japan. We thank Dr. Kiriko Kashiwakura, Japan Automobile Research Institute, and Dr. Shinichiro Okayama, Nissan Motor Co. Ltd., for providing the emission factor data derived from automobiles in Japan.

■ REFERENCES

(1) Agency for Toxic Substances and Disease Registry. *Toxicological Profile for Polycyclic Aromatic Hydrocarbons (PAHs)*; U.S. Department of Health and Human Service, Public Health Service: Atlanta, GA, 1995; www.atsdr.cdc.gov/ToxProfile/tp69.pdf.

(2) Xu, S.; Liu, W.; Tao, S. Emission of polycyclic aromatic hydrocarbons in China. *Environ. Sci. Technol.* **2006**, *40*, 702−708, DOI: 10.1021/es0517062.

(3) Zhang, Y. X.; Tao, S. Global atmospheric emission inventory of polycyclic aromatic hydrocarbons (PAHs) for 2004. *Atmos. Environ.* **2009**, *43*, 812−819, DOI: 10.1016/j.atmosenv.2008.10.050.

(4) Ravindra, K.; Sokhi, R.; Grieken, R. V. Atmospheric polycyclic aromatic hydrocarbons: Source attribution, emission factors and regulation. *Atmos. Environ.* **2008**, *42*, 2895−2921, DOI: 10.1016/j.atmosenv.2007.12.010.

(5) Tang, N.; Hattori, T.; Taga, R.; Igarashi, K.; Yang, X.; Tamura, K.; Kakimoto, H.; Mishukov, V. F.; Toriba, A.; Kizu, R.; Hayakawa, K. Polycyclic aromatic hydrocarbons and nitropolycyclic aromatic hydrocarbons in urban air particulates and their relationship to emission sources in the Pan-Japan Sea countries. *Atmos. Environ.* **2005**, *39*, 5817−5826, DOI: 10.1016/j.atmosenv.2005.06.018.

(6) Yang, X.-Y.; Okada, Y.; Tang, N.; Matsunaga, S.; Tamura, K.; Lin, J.-M.; Kameda, T.; Toriba, A.; Hayakawa, K. Long-range transport of polycyclic aromatic hydrocarbons from China to Japan. *Atmos. Environ.* **2007**, *41*, 2710−2718, DOI: 10.1016/j.atmosenv.2006.11.062.

(7) Hattori, T.; Tang, N.; Tamura, K.; Hokoda, A.; Yang, X.; Igarashi, K.; Ohno, M.; Okada, Y.; Kameda, T.; Toriba, A.; Hayakawa, K. Particulate polycyclic aromatic hydrocarbons and their nitrated derivatives in three cities in Liaoning Province, China. *Environ. Forensics.* **2007**, *8*, 165−172, DOI: 10.1080/15275920601180701.

(8) Zhang, Y.; Tao, S.; Shen, H.; Ma, J. Inhalation exposure to ambient polycyclic aromatic hydrocarbons and lung cancer risk of Chinese population. *Proc. Natl. Acad. Sci. U. S. A.* **2009**, *106*, 21063−21067, DOI: 10.1073/pnas.0905756106.

(9) Gusev, A.; Dutchak, S.; Rozovskaya, O.; Shatalov, V.; Sokovykh, V.; Vulykh, N.; Aas, W.; Breivik, K. *Persistent Organic Pollutants in the environments*; EMEP Status Report 3/2011; Meteorological Synthesizing Centre-East: Moscow, Russia, 2011; www.msceast.org/reps/3_2011.pdf (accessed April 2, 2012).

(10) Tsibulsky, V.; Sokolovsky, V.; Dutchak, S.; Shatalov, V. *MSC-E Contribution to the HM and POP Emission Inventories: Polycyclic Aromatic Hydrocarbon Emission Inventories and Emission Expert Estimates; Expert Estimates of Heavy Metal Emissions for some European Countries for 1980−98*; Technical Note 7/2001; Meteorological Synthesizing Centre-East: Moscow, 2001; www. msceast.org/index.php?option=com_content&view=article&id=27&Itemid=39#2001 (accessed April 2, 2012).

(11) Pacyna, J. M.; Breivik, K.; Munch, J.; Fudala, J. European atmospheric emissions of selected persistent organic pollutants, 1970−1995. *Atmos. Environ.* **2003**, *37-S1*, S119−S131, DOI: 10.1016/S1352-2310(03)00240-1.

(12) U.S. Environmental Protection Agency. *1990 Emission inventory of Section 112(c) (6) Pollutants: Polycyclic Organic Matter (POM), TCDD, TCDF, PCBs, Hexachlorobenzene, Mercury, and Alkylated Lead*, Final Report, Emission Factor and Inventory Group (MD-14), Emissions Monitoring and Analysis Division; Visibility and Ecosystem Protection Group (MD-15), Air Quality Strategies and Standards Division; United States Environmental Protection Agency: Research Triangle Park, NC, 1998; www.epa.gov/ttn/atw/112c6/final2.pdf (accessed April 2, 2012).

(13) Wenborn, M. J.; Coleman, P. J.; Passant, N. R.; Lymberidi, E.; Sully, J.; Weir, R. A. *Speciated PAH Inventory for the UK*, AEAT-3512/REMC/20459131/Issue 1; AEA Technology Environment: Oxford, UK,1999; http://uk-air.defra.gov.uk/reports/cat08/0512011419_REPFIN_all_nov.pdf (accessed April 2, 2012).

(14) Zhang, Y.; Dou, H.; Chang, B.; Wei, Z.; Qiu, W.; Liu, S.; Liu, W.; Tao, S. Emission of Polycyclic aromatic hydrocarbons from indoor straw burning and emission inventory updating in China. *Ann. N. Y. Acad. Sci.* **2008**, *1140*, 218−227, DOI: 10.1196/annals.1454.00.

(15) Liu, S.; Tao, S.; Liu, W.; Liu, Y.; Dou, H.; Zhao, J.; Wang, L.; Wang, J.; Tian, Z.; Gao, Y. Atmospheric polycyclic aromatic hydrocarbons in north China: A winter-time study. *Environ. Sci. Technol.* **2007**, *41*, 8256−8261, DOI: 10.1021/es0716249.

(16) Lang, C.; Tao, S.; Zhang, G.; Fu, J.; Simonich, S. Outflow of polycyclic aromatic hydrocarbons from Guangdong, Southern China. *Environ. Sci. Technol.* **2007**, *41*, 8370−8375, DOI: 10.1021/es071853v.

(17) Zhang, Y.; Shen, H.; Tao, S.; Ma, J. Modeling the atmospheric transport and outflow of polycyclic aromatic hydrocarbons emitted from China. *Atmos. Environ.* **2011**, *45*, 2820−2827, DOI: 10.1016/j.atmosenv.2011.03.006.

(18) Ohara, T.; Akimoto, H.; Kurokawa, J.; Horii, N.; Yamaji, K.; Yan, X.; Hayasaka, T. An Asian emission inventory of anthropogenic emission sources for the period 1980−2020. *Atmos. Chem. Phys.* **2007**, *7*, 4419−4444.

(19) Kajino, M.; Inomata, Y.; Sato, K.; Kurokawa, J.; Ohara, T.; Tang, N.; Hayakawa, K.; Ueda, H. Modeling polycyclic aromatic hydrocarbons over Northeast Asia using MRI-PM/p.(in preparation).

(20) U.S. Environmental Protection Agency. *Needs Assessment for U.S. EPA's Integrated Risk Information System*, EPA/635/R-02/004; National Center for Environmental Assessment, Office of Research and Developlment, United States Environmental Protection Agency: Washington, DC, 2003; www.epa.gov/iris/pdfs/iris_needs.pdf (accessed April 2, 2012).

(21) Streets, D. G.; Bond, T. C.; Carmichael, G. R.; Fernandes, S. D.; Fu, Q.; He, D.; Klimont, Z.; Nelson, S. M.; Tsai, N. Y.; Wang, M. Q.; Woo, J.-H.; Yarber., K. F. An inventory of gaseous and primary aerosol emissions in Asia in the year 2000. *J. Geophys. Res.* **2003**, *108*, 8809 DOI: 10.1029/2002JD003093.

(22) Carmichael, G. R.; Sakurai, T.; Streets, D.; Hozumi, Y.; Ueda, H.; Park, S. U.; Fung, C.; Han, Z.; Kajino, M.; Engardt, M.; Bennet, C.; Hayami, H.; Sartelet, K.; Holloway, T.; Wang, Z.; Kannari, A.; Fu, J.; Matsuda, K.; Thongboonchoo, N.; Amann, M. MICS-AsiaII: The model intercomparison study for Asia Phase II methodology and overview of findings. *Atmos. Environ.* **2008**, *42*, 3468−3490, DOI: 10.1016/j.atmosenv.2007.04.007.

(23) Giglio, L.; Randerson, J. T.; Van der Werf, G. R.; Kasibhatla, P. S.; Collatz, G. J.; Morton, D. C.; DeFries, R. S. Assessing variability and long-term trends in burned area by merging multiple satellite fire products. *Biogeosci.* **2010**, *7*, 1171−1186, DOI: 10.5194/bg-7-1171-2010.

(24) Yang, H.-H.; Lee, W.-J.; Chen, S.-J.; Lai, S.-O. PAH emission from various industrial stacks. *J. Hazard. Mater.* **1998**, *60*, 159−174.

(25) Li, C.-T.; Mi, H.-H.; Lee, W.-J.; You, W.-C.; Wang, Y.-F. PAH emission from the industrial boilers. *J. Hazard. Mater.* **1999**, *A69*, 1−11.

(26) Yan, J.-H.; You, X.-F.; Li, X.-D.; Ni, M.-J.; Yin, X.-F.; Cen, K.-F. Performance of PAHs emission from bituminous coal combustion. *J. Zhejiang Univ. Sci.* **2004**, *5*, 1554−1564, DOI: 10.1631/jzus.2004.1554.

(27) Chen, Y.; Bi, X.; Mai, B.; Sheng, G.; Fu, J. Emission characterization of particulate/gases and size association for polycyclic aromatic hydrocarbons from residential coal combustion. *Fuel.* **2004**, *83*, 781−790, DOI: 10.1016/j.fuel.2003.11.003.

(28) Chen, Y.; Sheng, G.; Bi, X.; Febg, Y.; Mai, B.; Fu, J. Emission factors for carbonaceous particles and polycyclic aromatic hydrocarbons from residential coal combustion in China. *Environ. Sci. Technol.* **2005**, *39*, 1861−1867, DOI: 10.1021/es0493650.

(29) Oanh, N. T. K.; Albina, D. O.; Ping, L.; Wang, X. Emission of particulate matter and polycyclic aromatic hydrocarbons from select cookstove-fuel systems in Asia. *Biomass. Bioenergy.* **2005**, *28*, 579−590, DOI: 10.1016/j.biombioe.2005.01.003.

(30) Kuo, C.-Y.; Lee, H-S; Lai, J.-H. Emission of polycyclic aromatic hydrocarbons and lead during Chinese mid-autumn festival. *Sci. Total Environ.* **2006**, *366*, 233−241, DOI: 10.1016/j.scitoenv.2005.08.006.

(31) Chen, Y.-C.; Sigh, P.-H. Emission of polycyclic aromatic hydrocarbons on the combustion of liquid crystal display components. *J. Environ. Eng.* **2006**, *132*, 1028−1033, DOI: 10.1061/(ASCE)0733-9372(2006)132:9(1028).

(32) Chen, S.-J.; Su, H.-B.; Chang, J.-E.; Lee, W.-J.; Huang, K.-L.; Hsieh, L.-T.; Huang, W.-J.; Lin, W.-Y.; Lin, C.-C. Emissions of polycyclic aromatic hydrocarbons (PAHs) from the pyrolysis of scrap

tires. *Atmos. Environ.* **2007**, *41*, 1209−1220, DOI: 10.1016/j.atmosenv.2006.09.041.

(33) Wang, H. L.; Zhuang, Y. H.; ZhengPin, H.; Cao, M.; Zhong, J. X.; Wang, X. K.; Oahn, N. T. K. Polycyclic aromatic hydrocarbons from rural household biomass burning in a typical Chinese village. *Sci. China. Ser. D-Earth Sci* **2008**, *51*, 1013−1020, DOI: 10.1007/s11430-008-0064-x.

(34) Yuan, H.; Tao, S.; Li, B.; Lang, C.; Cao, J.; Coveney, R. M. Emission and outflow of polycyclic aromatic hydrocarbons from wildfires in China. *Atmos. Environ.* **2008**, *42*, 6828−6835, DOI: 10.1016/j.atmosenv.2008.05.033.

(35) Wang, B.-G.; Lu, W.-M.; Zhou, Y.; Shao, M.; Zhang, Y.-H. Emission characteristic of PAHs composition in motor vehicles exhaust of city tunnel. *China Environ. Sci.* **2007**, *27*, 482−487.

(36) Kashiwakura, K.; Sasaki, S.; Nakajima, T.; Sakamoto, K. Emissions of regulated and non-regulated air pollutants emitted from heavy-duty diesel vehicles and their emission tendencies. *J. Soc. Atmos. Environ.* **2008**, *43*, 67−78.

(37) Chien, Y.-C.; Liang, C. P.; Shih, P. H. Emission of polycyclic aromatic hydrocarbons from the pyrolysis of liquid crystal wastes. *J. Hazard. Mater.* **2009**, *170*, 910−914, DOI: 10.1016/j.hazmat.2009.05.054.

(38) Etiope, G.; Iversen, N.; Woodfield, M.; Winiwarter, W. *EMEP/EEA Air Pollutant Emission Inventory Guidebook 2009; EEA Technical Report, ISSN 1725-2237*; European Environment Agency: Copenhagen, 2009; www.eea.europa.eu/publications/emep-eea-emission-inventory-guidebook-2009 (accessed April 2, 2012).

(39) Ho, K. F.; Ho, S. S. H.; Lee, S. C.; Cheng, Y.; Chow, J. C.; Watson, J. G.; Louie, P. K. K.; Tian, L. Emissions of gas- and particle-phase polycyclic aromatic hydrocarbons (PAHs) in the Shing Mun Tunnel, Hong Kong. *Atmos. Environ.* **2009**, *43*, 6343−6351, DOI: 10.1016/j.atmosenv.2009.09.025.

(40) Lu, H.; Zhu, L.; Zhu, N. Polycyclic aromatic hydrocarbon emission from straw Burning and the influence of combustion parameters. *Atmos. Environ.* **2009**, *43*, 978−983, DOI: 10.1016/j.atmosenv.2008.10.022.

(41) Liu, W. X.; Dou, H.; Wei, Z. C.; Chang, B.; Qiu, W. X.; Liu, Y.; Tao, S. Emission characteristics of polycyclic aromatic hydrocarbons from combustion of different residential coals in North China. *Sci. Total Environ.* **2009**, *407*, 1436−1446, DOI: 10.1016/j.scitotenv.2008.10.055.

(42) Kashiwakura, K.; Sasaki, S.; Sakamoto, K. Emissions of regulated and non-regulated air pollutants emitted from gasoline vehicles and their emission tendencies. *J. Soc. Atmos. Environ.* **2009**, *44*, 102−116.

(43) Shen, G.; Yang., Y.; Wang, W.; Tao., S.; Zhu., C.; Min, Y.; Xue., M.; Ding, J.; Wang., B.; Wang, R.; Shen, X.; Li, W.; Wang, X.; Russell, A. Emission factors of particulate matter and elemental carbon for crop residues and coals burned in typical household stoves in China. *Environ. Sci. Technol.* **2010**, *44*, 7157−7162, DOI: 10.1021/es101313y.

(44) Cao, G. L.; Zhang, X. Y.; Wang, Y; Zheng, F. Estimation of emissions from field burning of crop straw in China. *Chin. Sci. Bull.* **2008**, *53*, 784−790, DOI: 10.1017/s11434-008-0145-4.

(45) Chan, D.; Song, T. Corrigendum to "Estimates of biomass burning emissions in Tropical Asia based on satellite-derived data" published in. *Atmos. Chem. Phys.* **2010**, *10*, 2335−2551.

(46) Cao, G.; Zhang, X.; Zheng, F. Inventory of black carbon and organic carbon emissions from China. *Atmos. Environ.* **2006**, *40*, 6516−6527, DOI: 10.1016/j.atmosenv.2006.05.070.

(47) Kajino, M.; Inomata, Y.; Sato, K.; Ueda, H.; Han, Z.; An, J.; Katata, G.; Deushi, M.; Maki, T.; Oshima, N.; Kurokawa, J.; Ohara, T.; Takami, A.; Hatakeyama, S. Development of an aerosol chemical transport model RAQM2 and predictiopns of Northeast Asian aerosol mass, size, chemistry, and mixing type. *Atmos. Chem. Phys. Discuss.*, submitted.

(48) An, J.; Ueda, H.; Wang, Z.; Matsuda, K.; Kajino, M.; Cheng, X. Simulations of monthly mean nitrate concentrations in precipitation over East Asia. *Atmos. Environ.* **2002**, *36*, 4159−4171.

(49) Han, Z.; Ueda, H.; Sakurai, T. Model study on acidifying wet deposition in East Asia during wintertime. *Atmos. Environ.* **2006**, *40*, 2360−2373, DOI: 10.1016/j.atmosenv.2005.12.017.

(50) Kajino, M.; Ueda, H.; Sato, K.; Sakurai, T. Spatial distribution of the source-receptor relationship of sulfur in Northeast Asia. *Atmos. Chem. Phys.* **2011**, *11*, 6475−6491, DOI: 10.5194/acp-11-6475-2011.

(51) Gusev, A.; Mantseva, E.; Shatalov, V.; Strukov, B. *Regional Multicomponent Model MSCE-POP, Technical report, 5/2005 June*; Meteorological Synthesizing Center-East, 2005; www.msceast.org/index.php?option=com_content&view=article&id=27&Itemid=39# 2005 (accessed April 2, 2012).

(52) *ARW Version 3 Modeling System User's Guide*; National Center for Atmospheric Research: Boulder, CO, 2009; www.mmm.ucar.edu/wrf/users/docs/arw_v3.pdf (accessed April 2, 2012).

(53) Hayakawa, K. Atmospheric Pollution and its countermeasure in East Asia from the viewpoint of polycyclic aromatic hydrocarbons. *J. Health Sci.* **2009**, *55*, 870−878.

(54) Inomata, Y.; Chiba, M.; Igarashi, Y.; Aoyama, M.; Hirose, K. Seasonal and spatial variations of enhanced gamma dose rates derived from ^{222}Rn progenies during precipitation in Japan. *Atmos. Environ.* **2007**, *41*, 8043−8057, DOI: 10.1016/j.atmosenv.2007.06.046.

(55) *The World Factbook*; United States Central Intelligence Agency: Washington, DC, 2011; www.cia.gov/library/publications/the-world-factbook/rankorder/2004rank.html (accessed April 2, 2012).

Gene 499 (2012) 326–331

Contents lists available at SciVerse ScienceDirect

Gene

journal homepage: www.elsevier.com/locate/gene

Short Communication

Cloning of two members of the calcitonin-family receptors from stingray, *Dasyatis akajei*: Possible physiological roles of the calcitonin family in osmoregulation

Nobuo Suzuki [a,*], Toshio Sekiguchi [b], Honoo Satake [b], Kanoko Kato [c], Yudai Nishiyama [c], Hideya Takahashi [c,d], Janine A. Danks [e], T. John Martin [f], Atsuhiko Hattori [g], Masaki Nakano [g], Makiko Kakikawa [h], Sotoshi Yamada [h], Maho Ogoshi [c], Susumu Hyodo [i], Yoko Yamaguchi [i], Vishwajit S. Chowdhury [j], Kazuichi Hayakawa [k], Hisayuki Funahashi [l], Tatsuya Sakamoto [c], Yuichi Sasayama [a]

[a] *Noto Marine Laboratory, Institute of Nature and Environmental Technology, Kanazawa University, Housu-gun, Ishikawa 927-0553, Japan*
[b] *Bioorganic Research Institute, Suntory Foundation for Life Sciences, Osaka, 618-8503, Japan*
[c] *Ushimado Marine Institute, Okayama University, Ushimado, Okayama 701-4303, Japan*
[d] *Institute of Science and Technology, Niigata University, Niigata 950-2181, Japan*
[e] *School of Medical Sciences, RMIT University, Bundoora 3083, Australia*
[f] *St. Vincent's Institute of Medical Research, 41 Victoria Parade, Fitzroy 3065, Australia*
[g] *Department of Biology, College of Liberal Arts and Sciences, Tokyo Medical and Dental University, Ichikawa-city, Chiba 272-0827, Japan*
[h] *Institute of Nature and Environmental Technology, Kanazawa University, Kanazawa-city, Ishikawa 920-1192, Japan*
[i] *Atmosphere and Ocean Research Institute, University of Tokyo, Kashiwa-city, Chiba 277-8564 Japan*
[j] *International Education Center, Faculty of Agriculture, Kyushu University, Fukuoka 812-8581, Japan*
[k] *Faculty of Pharmaceutical Science, Institute of Medical, Pharmaceutical and Health Sciences, Kanazawa University, Kanazawa-city, Ishikawa 920-1192, Japan*
[l] *Showa University, School of Medicine, Department of Anatomy, Shinagawa-ku, Tokyo 142-8555, Japan*

ARTICLE INFO

Article history:
Accepted 4 March 2012
Available online 13 March 2012

Keywords:
Calcitonin
Calcitonin gene-related peptide
Tissue expression
Elasmobranch

ABSTRACT

In cartilaginous fish, two cDNAs encoding calcitonin-family receptors were isolated for the first time from the stingray brain. The open reading frame of one receptor cDNA coded a 525-amino acid protein. The amino acid identity of this receptor to human calcitonin-receptor-like receptor (CRLR) is 64.5%, frog CRLR is 64.7%, and flounder CRLR is 61.2% and this was higher than to human calcitonin receptor (CTR) (46.1%), frog CTR (54.7%), and flounder CTR (48.9%). We strongly suggested that this receptor is a ray CRLR based on phylogenetic analysis. In case of the second receptor, amino acid identity among CRLRs (human 50.5%, frog 50.7%, flounder 48.0%) and CTRs (human 43.2%, frog 49.1%, flounder 41.8%) was similar. From phylogenetic analysis of both CRLRs and CTRs, we believe that this receptor is ray CTR. The expression of ray CRLR mRNA was predominantly detected in the nervous system (brain) and vascular system (atrium, ventricle, and gill), which reflects the similar localization of CGRP in the nervous and vascular systems as mammals. It was observed that the second receptor was expressed in several tissues, namely cartilage, brain, pituitary gland, gill, atrium, ventricle, pancreas, spleen, liver, gall bladder, intestine, rectal gland, kidney, testis and ovary. This localization pattern was very similar to flounder CTR. Both receptor mRNAs were strongly expressed in the gill. This suggests that the calcitonin-family members are involved in the osmoregulation of stingray as this fish is known to be euryhaline. When a stingray was transferred to diluted seawater (20% seawater), the expression of both receptors significantly decreased in the gill. Similar results were obtained in the kidney of the stingray. Thus, our cloning and isolation of both receptors in the stingray will be helpful for elucidation of their physiological role(s) such as osmoregulation including calcium metabolism of cartilaginous fish.

1. Introduction

Calcitonin gene-related peptide (CGRP) is a 37 amino acid hormone whose mRNA is co-encoded with calcitonin (CT) mRNA on a single gene (Amara et al., 1982). In mammals, the mRNA synthesis of two hormones is controlled by tissue-specific alternative splicing; CGRP precursor mRNA is synthesized in the neural tissues; CT precursor mRNA is synthesized in the thyroidal C-cells (Rosenfeld et al., 1983). Since CGRP exists widely in the central nervous system

Abbreviations: bp, base pair(s); cDNA, DNA complementary to RNA; CGRP, calcitonin gene-related peptide; CT, calcitonin; CTR, calcitonin receptor; CRLR, calcitonin-receptor-like receptor; mRNA, messenger RNA; PCR, polymerase chain reaction; RACE, rapid amplification of cDNA ends; RT-PCR, reverse transcription-polymerase chain reaction.

* Corresponding author at: Noto Marine Laboratory, Institute of Nature and Environmental Technology, Kanazawa University, Ogi, Noto-cho, Ishikawa 927-0553, Japan. Tel.: +81 768 74 1151; fax: +81 768 74 1644.
E-mail address: nobuos@staff.kanazawa-u.ac.jp (N. Suzuki).

0378-1119/$ – see front matter © 2012 Elsevier B.V. All rights reserved.
doi:10.1016/j.gene.2012.03.042

(Gibson et al., 1984; Rosenfeld et al., 1983), it is suggested that CGRP plays role as a neuromediator or neuromodulator (Lafont et al., 2007). In addition, CGRP is synthesized in the heart and blood vessels to control blood flow by its potent vasodilatory actions (Brain and Grant, 2004; Mulderry et al., 1985; Wimalawansa, 1997).

In teleosts, the presence of CGRP immunoreactive substances has been demonstrated in trout (Fouchereau-Peron et al., 1990). Jansz and Zandberg (1992) characterized the CGRP gene of salmon, suggesting that salmon CGRP is the product of the alternative splicing of the CT/CGRP gene, common to mammals. We also cloned a part of genomic DNA including the CGRP gene from flounder (*Paralichthys olivaceus*) and detected mRNA expression in the brain and heart (Suzuki et al., 2001), suggesting that CGRP acts as a neuropeptide and a vasodilator in fish as well as mammals, as CGRP immunoreactivity has been detected in the brain of small-spotted dogfish (Molist et al., 1995), and may be quite important in homeostasis in all fish including cartilaginous fish (Lafont et al., 2007). On the other hand, calcitonin receptor-like receptor (CRLR) functions to a receptor for CGRP when it is co-expressed with RAMP1 (Husmann et al., 2000; McLatchie et al., 1998; Sexton et al., 2001). The distribution and expression analysis of CRLR under various physiological and environmental conditions could contribute to the understanding of physiological functions of CGRP in cartilaginous fish.

To study the physiological role of CGRP in cartilaginous fish, the full coding region of CRLR was sequenced from the brain of stingray and the mRNA expression in the various tissues was analyzed. In the process of CRLR cloning, a second member of the calcitonin-family receptors was isolated and cloned. Based on the data of multiple alignment, phylogenetic analysis and tissue distribution pattern, it is apparent that this receptor is equivalent to the stingray calcitonin receptor (CTR). In addition, it was found that the expression of two receptors was decreased in the gill and kidney when the rays were transferred to diluted seawater. Thus, this is the first study that identifies two members of calcitonin-family receptors in cartilaginous fish and indicates the possible physiological roles of CT and CGRP in the osmoregulation of stingray.

2. Materials and methods

2.1. Animals

The brain of male stingray (*Dasyatis akajei*) was used for PCR amplification. Male and female stingrays were used for the analysis of tissue-specific expression and adaptation in seawater. The original concentration of seawater (100%) and diluted seawater (20%) were used for this study. The animals were anesthetized with ethyl 3-amino-benzoate, methanesulfonic acid salt (Sigma-Aldrich Inc., MO, USA) and then dissected for tissue preparation.

All experimental procedures were conducted in accordance with the Guide for the Care and Use of Laboratory Animals prepared by Kanazawa University.

2.2. PCR amplification

Total RNAs were prepared using a total RNA isolation kit (Nippon Gene, Tokyo, Japan) from the brains of stingray. RT-PCR was performed using Oligotex-dT 30 Super (Takara, Kusatsu, Japan) as an oligo dT primer to prevent genomic DNA contamination (Suzuki et al., 1997). The PCR primers were designed at the well-conserved region of the mammalian CRLR and CTR cDNA sequences (Fig. 1). The primer sequences were 5′-1:GYAAYMGXACXTGGGAYGG, 5′-2: GAYTAYTTYCCXGAYTTYGA, 3′-1:CCYTCRCAXARCATCCARAA, and 3′-2:CATCCARAARTARTTRCA (Suzuki et al., 2000). The 1st and the nested-PCR (1st PCR: 5′-1/3′-1 primer set; 2nd PCR: 5′-2/3′-2 primer set) were performed using a *Taq* polymerase and an additional buffer (Takara Bio Inc., Otsu, Japan). The PCR parameters were 35 cycles of 96 °C for 30 s, 45 °C for 1 min, and 72 °C for 2 min. The sequencing of the PCR products of the expected length (422 bp) was performed by Dragon Genomics Center, Takara Bio Inc. (Mie, Japan).

2.3. RACE amplification of receptors cDNAs in stingray

Total RNA (1 μg) was obtained from the stingray brain. The complete sequences of the two receptors were obtained by 5′- and 3′-RACE method using a kit 5′ RACE System, Version 2.0 and 3′ RACE System for Rapid Amplification of cDNA Ends, respectively (Invitrogen, CA, USA). The primer locations for two receptors were described in supplementary figures. RACE was performed using the respective gene-specific primer and the primer of adaptor sequences in the kit. The products were sequenced on an ABI PRISM 3130 sequencer (Applied Biosystems, CA, USA) using BigDye terminators.

2.4. Expression analysis

Total RNAs were prepared from the cartilage, brain, pituitary gland, gill atrium, ventricle, pancreas, spleen, liver, gall bladder, intestine, rectal gland, kidney, and testis of male stingray, as well as the ovary of female stingray using a total RNA isolation kit (Nippon Gene). RT-PCR was performed using the primer set (CRLR 5′: AGACTTCGATCCATCAGA, CRLR 3′: AGTCAATGCTGTCTTTA, CTR-like

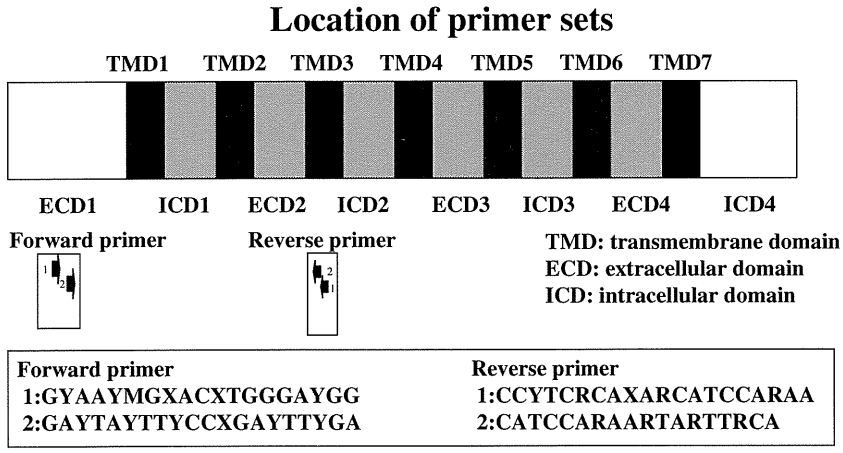

Fig. 1. Location and sequence of primers. The CRLR and CTR molecules have four extracellular domains (Ecd) 1–4, seven transmembrane domains (Tmd 1–7), and for intracellular domains (Icd 1–4). The PCR primers were designed to the highly conserved region of the mammalian CRLR and CTR cDNA sequences.

5′: CACGGAAAAGGTCACC, CTR-like 3′: AGTGAACAAAGAGTAATAT). The conditions for PCR amplification were 40 cycles of denaturation for 0.5 min at 96 °C, annealing for 1 min at 60 °C, and extension for 2 min at 72 °C, followed by a single cycle at 72 °C for 30 min. In case of the β-actin cDNA (AB675482), the amplification using a primer set (5′: TTGGCAATGAGCGATTCAGA; 3′: CACAGGATTCCATACCCAAGAAA) were consisted of 25 cycles of denaturation for 0.5 min at 96 °C, annealing for 1 min at 60 °C, and extension for 2 min at 72 °C, followed by a single cycle at 72 °C for 15 min. The PCR products were analyzed on 2.5% NuSive GTG agarose gel (FMC Bioproducts, ME, USA) and stained with ethidium bromide.

2.5. Phylogenetic analysis

The amino acid sequences were aligned using the CLUSTAL program (Higgins and Sharp, 1988). After removing gaps, the verified alignments were used to construct phylogenetic trees. The trees were calculated using MEGA program based on the neighbor-joining method (Kumar et al., 2001; Saitou and Nei, 1987). The sequences used were as follows: Human-CRLR, NP_005786; Pig-CRLR, Q867C1; Dog-CRLR, XP_545560; Mouse-CRLR, NP_061252; Xenopus-CRLR, NP_001016893; Fugu-CRLR2, BAE45313; Salmon-CRLR, CAD48406; Flounder-CRLR, AB035314; Fugu-CRLR1, BAE45312; Flounder-CTR, AB035315; Chicken-CTR, XP_425985; Bullfrog-CTR, Q28DX2; Fugu-CTR, BAE76018; Medaka-CTR, AAI19273; Pig-CTR, AAA31023; Mouse-CTR, AAI19273; Human-CTR, NP_001733; Dog-CTR, XP_539423; Ascidian-CTR, BAI63096; Human-CRHR1, NP_004373.

2.6. Analysis of the mRNA expression of both ray CRLR and CTR-like receptors in the gill and kidney after transfer to diluted seawater

Seawater adapted-stingrays ($n=8$, both sexes) were gradually transferred into diluted seawater. In the first day, the stingrays were transferred to 80% seawater and then kept for 6 hours followed by putting them into 60% seawater for remaining of the day. In the next day, the stingrays were kept in 40% seawater for 6 hours, and then transferred into 20% seawater. After keeping the stingrays in 20% seawater for 12 hours, the stingrays were anesthetized with ethyl 3-aminobenzoate, methanesulfonic acid salt (Sigma-Aldrich). The gill and kidney were collected from stingray under proper anesthetic condition. Also, the seawater-adapted stingrays ($n=8$, both sexes) were anesthetized with ethyl 3-aminobenzoate, methanesulfonic acid salt (Sigma-Aldrich). The gill and kidney were removed from the seawater stingrays.

Total RNA was prepared using a total RNA isolation kit for fibrous tissue and complementary DNA synthesis was performed (RNase Easy Fibrous Mini-Kit, Qiagen GmbH, Hilden, Germany). The real-time PCR amplification was analyzed with a Bio-Rad iCycler (Bio-Rad, Hercules, CA) using the primers for CRLR (5′: GGAGAAGCTAAAGACAGCATTGACT; 3′: CAGCAGCGAAGCCACTGATA′) and for CTR-like (5′: GGAAAAGGTCACCAAGATTTGC; 3′: AGTCCATGTTCGGTTGCTCTCT). The annealing temperature in the amplification of both CRLR and CTR-like cDNAs was 63 °C. The amplified PCR products have been verified by sequencing to confirm its sequences. The detailed conditions of PCR were described in our previous study (Takahashi et al., 2007). The CRLR and CTR-like mRNA levels were normalized to the β-actin mRNA level measured by above described primer set (5′: TTGGCAATGAGCGATTCAGA; 3′: CACAGGATTCCATACCCAAGAAA).

2.7. Statistical analysis

Real-time PCR was performed and the data were analyzed using the Student's t-test. The significance level was $P<0.05$.

3. Results and discussion

3.1. PCR amplification of two receptors in the brain of stingray

Sequence analysis indicated that two types of cDNA fragments are amplified by PCR primer sets at the conserved regions of mammalian CRLR and CTR cDNA sequences. One cDNA fragment (422 bp) had high identity to flounder CRLR (73.4%) and human CRLR (81.3%) and to a lesser extent to flounder CTR (53.9%) and human CTR (56.3%). The second cDNA (422 bp) had high identity to both CRLR (to human 57.0%; to flounder 48.3%) and CTR (to human 59.4%; to flounder 63.3%). Thus, we believe that two receptors belong to the calcitonin-family receptors.

3.2. RACE cloning and sequencing of two calcitonin-family receptors

By RACE cloning, the full sequences of the two calcitonin-family receptors were determined. The open reading frame of one receptor cDNA coded a 525-amino acid protein (see Supplementary data). The amino acid identity of this receptor to CRLR was highest with human CRLR (64.5%), frog (64.7%), and flounder (61.2%) and this was higher than the CTR of human (46.1%), frog (54.7%), or flounder (48.9%). This strongly suggested that the obtained cDNA encodes CRLR in stingray.

The amino acid identity of the second stingray receptor (see Supplementary data) was similar to CRLRs (human 50.5%, frog 50.7%, flounder 48.0%) and CTRs of other species (human 43.2%, frog 49.1%, flounder 41.8%). After alignment of flounder CRLR, flounder CTR, human CRLR, human CTR, and two stingray receptors, three potential sites (Asn-X-Ser/Thr) for N-linked glycosylation, which are conserved in mammalian CRLR and CTR, were identified in stingray receptors before the first putative transmembrane domain. Furthermore, 12 cysteines were conserved among CRLRs, CTRs, and stingray receptors. These glycosylation sites and cysteines are suggested to be important for ligand binding (Ho et al., 1999; Qi et al., 1997). Using BLAST against the DDBJ/NCBI protein database, furthermore, we confirmed that the sequences are most similar to CRLR and CTR. Thus, we concluded that two receptors belong to the calcitonin-family receptors.

3.3. Phylogenetic analysis of calcitonin-family receptors

The phylogenetic tree was determined for the known calcitonin-family receptors together with stingray receptors (see Supplementary data). As a result, the stingray receptors were located with CRLR and CTR in other animals. The first stingray receptor branched from teleost CRLR and composed of a clade of mammalian and xenopus CRLR. This result strongly supports that the amino acid sequence was that of stingray CRLR (ray CRLR). The second stingray receptor co-located with flounder CTR and was placed between the CRLRs clade and the non-mammalian CTRs clade (see Supplementary data).

We previously reported amino acid sequences of both CT and CGRP in flounder (Suzuki et al., 2001). The amino acid sequence of flounder CT was more similar to teleosts (78–100%), salamander (81%), reptiles (84%), and chicken (84%) than those of stingray (72%) and frogs (56–78%), and it is largely different from that of mammals (31–50%). However, the predicted amino acid sequence of flounder CGRP was more conserved than CT among vertebrates and showed 78%, 78%, 78%, 81%, and 73–78% identity to salmon, cod, frog, chicken, and mammalian CGRPs, respectively. Among vertebrates, CGRP is a well-conserved molecule during evolution while CT is quite varied. Corresponding to sequence changes in ligand (CT), the receptor (CTR) seems to be varied largely. Thus, it is highly likely that the second receptor is the stingray equivalent of CTR (ray CTR-like).

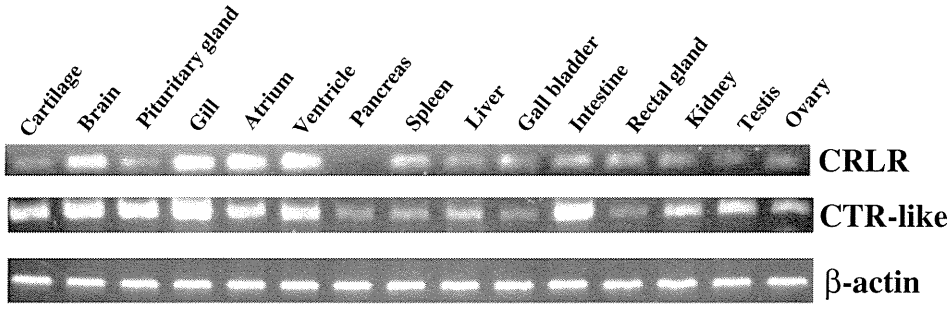

Fig. 2. Tissue specific expression of ray CRLR and ray CTR-like mRNAs by RT-PCR. After PCR amplification, the PCR products were analyzed on 2.5% NuSive GTG agarose gel (FMC Bioproducts, ME, USA) and stained with ethidium bromide.

3.4. Expression of ray CRLR and ray CTR-like mRNAs in different tissues

Specific PCR products of ray CRLR mRNA were amplified from brain, gill, atrium and ventricle and detected in cartilage, pituitary gland, spleen, liver, gall-bladder, intestine, rectual gland, kidney, testis and ovary (Fig. 2). Pancreas did not show any expression with the present conditions (Fig. 2). The ray CRLR mRNA expression was found in brain, heart and intestine and this was the same as seen in mammals (Eysselein et al., 1991; Poyner, 1992), suggesting similar functions in those tissues. In spleen, relatively high expression of ray CRLR was detected. Arlot-Bonnemains et al. (1991) reported that CGRP-specific binding in trout tissues is high in the spleen although the function has not yet been elucidated. In the early development of gut in zebrafish, the number of nerve cell bodies and fibers gradually increased and CGRP was detected in these nerve cells (Olsson et al., 2008). In another study, cod CGRP (10^{-9}–10^{-7} M) inhibited the motility of spontaneously active ring preparations from the cod intestine (Shahbazi et al., 1998) suggesting that CGRP plays a role in fish gut development and physiology. The localization of CGRP in the stingray gut suggests that CGRP may have significant roles in its gut.

Recently, involvement of CGRP in the outgrowth of the gubernaculums has been noted, and it has been suggested to play a role in testicular descent in mammalians (Chan et al., 2009). CGRP released from the genitofemoral nerve causes maximal mitosis in the gubernacular bulb of mammals (Chan et al., 2009). In stingray, this hormone may involve in testicular development that regulates the balance between cell proliferation and apoptosis.

Specific PCR products of ray CTR-like mRNA were amplified from cartilage, brain, pituitary gland, gill, atrium, ventricle, pancreas, spleen, liver, gall bladder, intestine, rectal gland, kidney, testis, and ovary (Fig. 2). In the cartilage of stingray, we detected ray CTR-like mRNA expression. It has been reported that CT acts on mammalian cartilage and promotes synthesis (Karsdal et al., 2006; Sondergaard et al., 2006). In the stingray, thus, CT may function to the growth of cartilage. CT-immunoreactive cells were found in the intestine of goldfish and appeared to control absorption of nutrients (Okuda et al., 1999). Therefore, the presence of ray CTR-like mRNA in intestine corresponds well with this physiological role of CT in fish. Previously mRNA expression of salmon CTR was detected in brain and pituitary gland and this was consistent with another study in mammalian tissues (Azria, 1989) where it was suggested that CT might act as a neurotransmitter.

In female sharks, it had been shown that plasma CT levels were elevated during reproductive periods (Nichols et al., 2003). We previously reported that estrogen-specific-binding and estrogen receptor mRNA were present in the stingray ultimobranchial gland (CT secreting organ in sub-mammalian vertebrates) (Yamamoto et al., 1996). The possible involvement of CT in stingray reproductive physiology is implied because of the presence of this receptor in the ovary and testis of stingray in the present study.

Ray CRLR and ray CTR-like mRNAs were found to be expressed in the excretory organs such as gill, kidney and rectal gland. As this fish is euryhaline (de Vlaming and Sage, 1973; Evans et al., 2010; Janech et al., 2003) and CGRP functions to osmoregulation in teleosts (Lafont et al., 2007; Lamharzi and Fouchereau-Peron, 1996; Suzuki

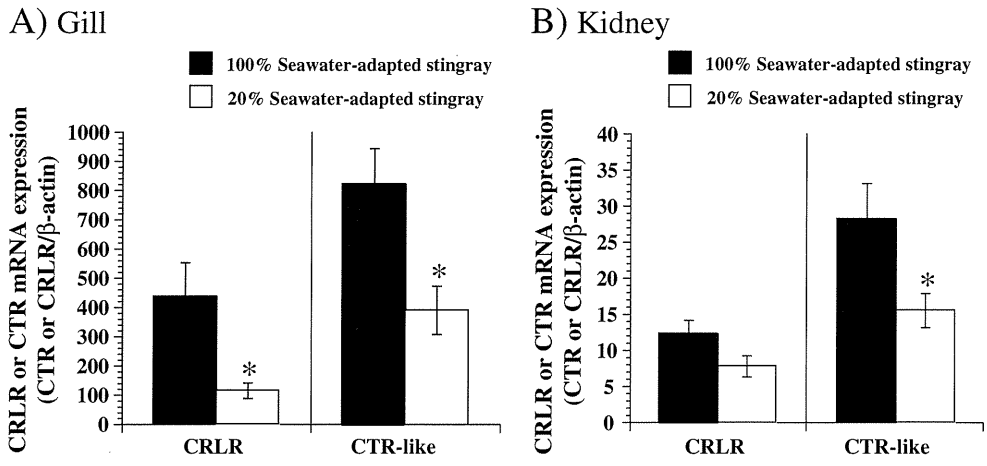

Fig. 3. Changes in mRNA expression of both ray CRLR and CTR-like receptors in the gill (A) and kidney (B) when transferred to diluted (20%) seawater. * indicates statistically significant difference at $P<0.05$ from the values in the control. The data were expressed as mean ± SEM ($n=8$).

et al., 2002), we examined ray CRLR and ray CTR-like mRNA expression in the gill and kidney when stingrays were transferred to the diluted seawater.

3.5. Changes in mRNA expression of both ray CRLR and CTR-like receptors in the gill and kidney when transferred to diluted seawater

The results are shown in Fig. 3. The ray CTR-like mRNA expression in the gill and kidney was higher than the ray CRLR mRNA. These results coincided with the tissue specific expressions (Fig. 2). When stingrays were transferred to the diluted seawater (20% seawater), both receptors mRNA expression significantly decreased in the gill. Similar results were obtained in the stingray kidney. When rainbow trout were adapted to seawater, their plasma CGRP levels and CGRP binding sites in the gill increased (Lamharzi and Fouchereau-Peron, 1996). Similarly when flounder were moved from seawater to freshwater, CRLR mRNA expression decreased (Suzuki et al., 2002). Thus, CGRP may play a role in osmoregulation in teleosts (Lafont et al., 2007).

Interestingly, the plasma level of CT did not change when freshwater adapted eels were moved to 100% seawater (Suzuki et al., 1999). This was reflected in the study where the flounder were transferred from seawater to freshwater and CTR mRNA expression in the gill did not alter (Suzuki et al., 2002). Therefore, CT may play a role in osmoregulation in cartilaginous fish and not in teleosts, as CT has some functions in osmoregulation as the CTR-like mRNA expression in both stingray gill and kidney was decreased when the fish were transferred from seawater to freshwater. Further study is required to elucidate the possible roles of CT and CGPR in cartilaginous fish.

3.6. Conclusions

(1) cDNA encoding CRLR was cloned from the stingray brain. Tissue-expression analysis, using RT-PCR, indicated that ray CRLR mRNA was detected mainly in the nervous system (brain) and vascular system (atrium, ventricle, and gill), indicating that CGRP may play roles in the nervous and vascular systems as it does in mammals.
(2) Another receptor cDNA was cloned from the brain of stingray. Based on the data of multiple alignments, phylogenetic analysis and tissue distribution pattern, this receptor is CTR equivalent in stingray.
(3) When stingray transferred to the diluted seawater (20% seawater), mRNA expression of both receptors was significantly decreased in the stingray gill. Similar results were obtained in the kidney. Thus, identification of two members of the calcitonin-family receptors in the stingray will assist in the elucidation of the physiological roles of these receptors and their ligands in cartilaginous fish.

Acknowledgments

This study was supported in part by grants to N.S. (Grant-in-Aid for Scientific Research (C) No. 21500404 by JSPS; Grant-in-Aid for Space Utilization by Japan Aerospace Exploration Agency), to A.H. (Grant-in-Aid for Scientific Research (C) No. 21570062 by JSPS), to T.S. (Grant-in-Aid for Scientific Research (C) No. 22570065 by JSPS), to M.O. (Grant-in-Aid for Encouragement of Scientists No. 22870020 by JSPS), and to K.H. [the Environment Research and Technology Development Fund (B-0905) by the Ministry of the Environment in Japan; Health and Labor Sciences Research Grants of Ministry of Health, Labor and Welfare, Japan; Grant-in-Aid for Scientific Research (B) No. 21390034 by JSPS]. This work was carried out in part as a joint-research in Japanese Association for Marine Biology (JAMBIO).

Appendix A. Supplementary Data

Supplementary data to this article can be found online at doi:10.1016/j.gene.2012.03.042.

References

Amara, S.G., Jonas, V., Rosenfeld, M.G., Ong, E.S., Evans, R.M., 1982. Alternative RNA processing in calcitonin gene expression generates mRNAs encoding different polypeptide products. Nature 298, 240–244.
Arlot-Bonnemains, Y., Fouchereau-Peron, M., Jullienne, A., Milhaud, G., Moukhtar, M.S., 1991. Binding sites of calcitonin gene related peptide (CGRP) to trout tissues. Neuropeptides 20, 181–186.
Azria, M., 1989. The Calcitonins: Physiology and Pharmacology. Karger, Basel.
Brain, S.D., Grant, A.D., 2004. Vascular actions of calcitonin gene-related peptide and adrenomedullin. Physiol. Rev. 84, 903–934.
Chan, J.J., Farmer, P.J., Southwell, B.R., Sourial, M., Hutson, J.M., 2009. Calcitonin gene-related peptide is a survival factor, inhibiting apoptosis in neonatal rat gubernaculum *in vitro*. J. Pediatr. Surg. 44, 1497–1501.
De Vlaming, V.L., Sage, M., 1973. Osmoregulation in the euryhaline elasmobranch, *Dasyatis Sabina*. Comp. Biochem. Physiol. 45A, 31–44.
Evans, A.N., Henning, T., Gelsleichter, J., Nunez, B.S., 2010. Molecular classification of an elasmobranch angiotensin receptor: quantification of angiotensin receptor and natriuretic peptide receptor mRNAs in saltwater and freshwater populations of the Atlantic stingray. Comp. Biochem. Physiol. 157B, 423–431.
Eysselein, V.E., et al., 1991. Structural characterization of calcitonin gene-related peptide purified from rabbit intestine. Peptides 12, 289–295.
Fouchereau-Peron, M., Arlot-Bonnemains, Y., Taboulet, J., Milhaud, G., Moukhtar, M.S., 1990. Distribution of calcitonin gene-related peptide and calcitonin-like immunoreactivity in trout. Regul. Pept. 27, 171–179.
Gibson, S.J., et al., 1984. Calcitonin gene-related peptide immunoreactivity in the spinal cord of man and of eight other species. J. Neurosci. 4, 3101–3111.
Higgins, D.G., Sharp, P.M., 1988. CLUSTAL: a package for performing multiple sequence alignment on a microcomputer. Gene 73, 237–244.
Ho, H.H., Gilbert, M.T., Nussenzveig, D.R., Gershengorn, M.C., 1999. Glycosylation is important for binding to human calcitonin receptors. Biochemistry 38, 1866–1872.
Husmann, K., Sexton, P.M., Fischer, J.A., Born, W., 2000. Mouse receptor-activity-modifying proteins 1, -2, and -3: amino acid sequence, expression and function. Mol. Cell. Endocrinol. 162, 35–43.
Janech, M.G., et al., 2003. Molecular and functional characterization of a urea transporter from the kidney of the Atlantic stingray. Am. J. Physiol. Renal Physiol. 284, F996–F1005.
Jansz, H.S., Zandberg, J., 1992. Identification and partial characterization of the salmon calcitonin/CGRP gene by polymerase chain reaction. Ann. N. Y. Acad. Sci. 657, 63–69.
Karsdal, M.A., et al., 2006. Calcitonin is involved in cartilage homeostasis: is calcitonin a treatment for OA? Osteoarthritis Cartilage 14, 617–624.
Kumar, S., Tamura, K., Jakobsen, I.B., Nei, M., 2001. MEGA2: molecular evolutionary genetics analysis software. Bioinformatics 17, 1244–1245.
Lafont, A.-G., Dufour, S., Fouchereau-Peron, M., 2007. Evolution of the CT/CGRP family: comparative study with new data from models of teleosts, the eel, and cephalopod molluscs, the cuttlefish and the nautilus. Gen. Comp. Endocrinol. 153, 155–169.
Lamharzi, N., Fouchereau-Peron, M., 1996. Adaptation of rainbow trout to seawater: changes in calcitonin gene-related peptide levels are associated with an increase in hormone-receptor interaction in gill membranes. Gen. Comp. Endocrinol. 102, 274–280.
McLatchie, L.M., et al., 1998. RAMPs regulate the transport and ligand specificity of the calcitonin-receptor-like receptor. Nature 393, 333–339.
Molist, P., Rodriguez-Moldes, I., Batten, T.F.C., Anadon, R., 1995. Distribution of calcitonin gene-related peptide-like immunoreactivity in the brain of the small-spotted dogfish, *Scyliorhinus canicula* L. J. Comp. Neurol. 352, 335–350.
Mulderry, P.K., et al., 1985. Calcitonin gene-related peptide in cardiovascular tissues of the rat. Neuroscience 14, 947–954.
Nichols, S., Gelsleichter, J., Manire, C.A., Cailliet, G.M., 2003. Calcitonin-like immunoreactivity in serum and tissues of the bonnethead shark, *Sphyrna tiburo*. J. Exp. Zool. A Comp. Exp. Biol. 298, 150–161.
Okuda, R., Sasyama, Y., Suzuki, N., Kambegawa, A., Srivastav, A.K., 1999. Calcitonin cells in the intestine of goldfish and a comparison of the number of cells among saline-fed, soup-fed, or high Ca soup-fed fishes. Gen. Comp. Endocrinol. 113, 267–273.
Olsson, C., Holmberg, A., Holmgren, S., 2008. Development of enteric and vagal innervation of the zebrafish (*Danio rerio*) gut. J. Comp. Neurol. 508, 756–770.
Poyner, D.R., 1992. Calcitonin gene-related peptide: multiple actions, multiple receptors. Pharmacol. Ther. 56, 23–51.
Qi, L.J., Leung, A.T., Xiong, Y., Marx, K.A., Abou-Samra, A.-B., 1997. Extracellular cysteines of the corticotropin-releasing factor receptor are critical for ligand interaction. Biochemistry 36, 12442–12448.
Rosenfeld, M.G., et al., 1983. Production of a novel neuropeptide encoded by the calcitonin gene via tissue-specific RNA processing. Nature 304, 129–135.
Saitou, N., Nei, M., 1987. The neighbor-joining method: a new method for reconstructing phylogenetic trees. Mol. Biol. Evol. 4, 406–425.
Sexton, P.M., Albiston, A., Morfis, M., Tilakaratne, N., 2001. Receptor activity modifying proteins. Cell. Signal. 13, 73–83.

Shahbazi, F., Karila, P., Olsson, C., Holmgren, S., Conlon, J.M., Jensen, J., 1998. Primary structure, distribution, and effects on motility of CGRP in the intestine of the cod *Gadus morhua*. Am. J. Physiol. Regul. Integr. Comp. Physiol. 275, R19–R28.

Sondergaard, B.C., et al., 2006. Calcitonin directly attenuates collagen type II degradation by inhibition of matrix metalloproteinase expression and activity in articular chondrocytes. Osteoarthritis Cartilage 14, 759–768.

Suzuki, N., Eguchi, C., Hirai, T., Sasayama, Y., 1997. Nucleotide sequences of reptile calcitonins: their high homology to chicken calcitonin. Zool. Sci. 14, 833–836.

Suzuki, N., Suzuki, D., Sasayama, Y., Srivastav, A.K., Kambegawa, A., Asahina, K., 1999. Plasma calcium and calcitonin levels in eels fed a high calcium solution or transferred to seawater. Gen. Comp. Endocrinol. 114, 324–329.

Suzuki, N., Suzuki, T., Kurokawa, T., 2000. Cloning of a calcitonin gene-related peptide receptor and a novel calcitonin receptor-like receptor from the gill of flounder, *Paralichthys olivaceus*. Gene 244, 81–88.

Suzuki, N., Suzuki, T., Kurokawa, T., 2001. Cloning of a calcitonin gene-related peptide from genomic DNA and its mRNA expression in flounder, *Paralichthys olivaceus*. Peptides 22, 1435–1438.

Suzuki, N., Suzuki, T., Kurokawa, T., 2002. Possible involvement of calcitonin gene-related peptide in seawater adaptation of flounder: expression analysis of its receptor mRNA in the gill. Fish. Sci. 68, 425–429.

Takahashi, H., et al., 2007. Prolactin receptor and proliferating/apoptotic cells in esophagus of the Mozambique tilapia (*Oreochromis mossambicus*) in fresh water and in seawater. Gen. Comp. Endocrinol. 152, 326–331.

Wimalawansa, S.J., 1997. Amylin, calcitonin gene-related peptide, calcitonin, and adrenomedullin: a peptide superfamily. Crit. Rev. Neurobiol. 11, 167–239.

Yamamoto, K., Suzuki, N., Takahashi, N., Sasayama, Y., Kikuyama, S., 1996. Estrogen receptors in the stingray (*Dasyatis akajei*) ultimobranchial gland. Gen. Comp. Endocrinol. 101, 107–114.

Bone 50 (2012) 1240–1249

Contents lists available at SciVerse ScienceDirect

Bone

journal homepage: www.elsevier.com/locate/bone

Original Full Length Article

Expression of osteoblastic and osteoclastic genes during spontaneous regeneration and autotransplantation of goldfish scale: A new tool to study intramembranous bone regeneration

Thiparpa Aime Thamamongood [a,b], Ryo Furuya [c,b], Shunsuke Fukuba [d,b], Masahisa Nakamura [c], Nobuo Suzuki [e], Atsuhiko Hattori [b,*]

[a] Undergraduate School of Medicine, Tokyo Medical and Dental University, Bunkyo-ku, Tokyo 113-8549, Japan
[b] Department of Biology, College of Liberal Arts and Sciences, Tokyo Medical and Dental University, Ichikawa-shi, Chiba 272-0827, Japan
[c] Department of Biology, Faculty of Education and Integrated Arts and Sciences, Waseda University, Shinjuku-ku, Tokyo 162-8480, Japan
[d] Undergraduate School of Dentistry, Tokyo Medical and Dental University, Bunkyo-ku, Tokyo 113-8549, Japan
[e] Noto Marine Laboratory, Institute of Nature and Environmental Technology, Kanazawa University, Noto-cho, Ishikawa 927-0553, Japan

ARTICLE INFO

Article history:
Received 7 December 2011
Revised 6 March 2012
Accepted 18 March 2012
Available online 29 March 2012

Edited by: T. Jack Martin

Keywords:
Osteoblastic genes
Osteoclastic genes
Teleost scale regeneration
Scale autotransplantation
Intramembranous bone regeneration
Cell-to-cell contact

ABSTRACT

Complementary DNA of osteoblast-specific genes (dlx5, runx2a, runx2b, osterix, RANKL, type I collagen, ALP, and osteocalcin) was cloned from goldfish (*Carassius auratus*) scale. Messenger RNA expressions were analyzed during spontaneous scale regeneration. Dlx5 had an early peak of expression on day 7, whereas osterix was constantly expressed during days 7–21. Runx2, a major osteoblastic transcription factor in mammalian bone, did not show any significant expression. The expressions of two functional genes, type I collagen and ALP, continually increased after day 7, while that of osteocalcin increased on day 14. As for osteoclastic markers, in addition to the cloning of two functional genes, TRAP and cathepsin K, in our previous study, we here cloned the transcription factor NFATc1 to use as an early osteoclastic marker. Using these bone markers, we investigate the signal key that controls the onset of scale resorption and regeneration by performing intra-scale-pocket autotransplantation of five groups of modified scales, namely, 1) methanol-fixed scale, 2) proteinase K-treated cell-free scale, 3) polarity reversal (upside-down) scale, 4) U-shape trimmed scale, and 5) circular-hole perforated scale. In this autotransplantation, each ontogenic scale was pulled out, modified, and then re-inserted into the same scale pocket. At post-transplant, inside the pockets of all modified transplant groups, new regenerating scales formed, attaching to the ongoing resorbed transplants. Autotransplantation of methanol-fixed scale, proteinase K-treated cell-free scale, and polarity reversal (upside-down) scale triggered scale resorption and scale regeneration. These two processes of scale resorption and regeneration occurred in accordance with osteoclastic and osteoblastic marker gene expressions. These results were microscopically confirmed using TRAP and ALP staining. Regarding the autotransplantation of U-shape trimmed and circular-hole perforated scales, new scales regenerated and grew at the trimmed/perforated part of each transplant, while scale resorption occurred apparently only around the trimmed/perforated area. In contrast, no scale resorption or regeneration was detected in sham transplantations. Our finding suggests that loss of correct cell-to-cell contact between the scale-pocket lining cells and the scale cortex cells is the key to switch on the onset of scale resorption and regeneration. Overall, the present study shows that goldfish scale regeneration shares similarities in gene expression with intramembranous bone regeneration. Improved understanding of goldfish scale regeneration will help elucidate the process of intramembranous bone regeneration and make goldfish scale a possible new tool to study bone regeneration.

Introduction

Teleost fish, a fish of a large group (division Teleostei) that comprises most bony fishes, has two main types of scales, cycloid and ctenoid. Cycloid scales are scales with a smooth surface. Fish such as goldfish and carp have cycloid scales. Ctenoid scales have tiny points on their surface and are found on fish such as bass and perch. Teleost scale has been shown to be a good model for studying bone metabolism [1–4]. It contains calcified tissue consisting of osteoblasts, osteoclasts, and bone matrix protein. The scale of teleost shares many characteristics with mammalian membrane bone. We previously reported morphological similarity between scale regeneration and membrane bone osteogenesis [2]. In the mentioned study, scale

* Corresponding author at: Department of Biology, College of Liberal Arts and Sciences, Tokyo Medical and Dental University, 2-8-30 Kounodai, Ichikawa, Chiba 272-0827, Japan. Tel./fax: +81 473 00 7126.
E-mail address: ahattori.las@tmd.ac.jp (A. Hattori).

8756-3282/$ – see front matter © 2012 Elsevier Inc. All rights reserved.
doi:10.1016/j.bone.2012.03.021

osteoblast appearance and activity were discussed by comparing to those in developmental study of mammalian membrane bone [5–9]. For osteoclast, we reported that scale osteoclasts create a ruffled border which is rich in mitochondria to increase the surface area interface for bone resorption. Mature osteoclasts in scales are multinucleated and express tartrate-resistant acid phosphatase (TRAP) and cathepsin K [1]. Recently, it was found that scale osteoblasts and osteoclasts are capable of responding to parathyroid hormone 1 (1–34) [10].

In fish skeletal tissue, a number of osteoblastic markers have been detected: alkaline phosphatase (ALP) [11]; runt related transcription factor 2 (runx2) [12]; and receptor activator of the NF-κB ligand (RANKL) [13]. In the scale of teleost, type I collagen is present in goldfish scale (*Carassius auratus*) [14]. Osterix expression has been observed in the scales of medaka (*Oryzias latipes*) [15]. Osteocalcin, a marker for mature bone matrix producing cells in mammals as well as teleost species [16–18], has been purified from scales of bluegill (*Lepomis macrochirus*) [19]. In zebrafish, osteocalcin mRNAs have been localized in all mineralized tissues during and after calcification, including bone and calcified cartilage of branchial arches [16]; however, to date, no research has been conducted to examine the pattern expression of osteocalcin during scale regeneration. Dlx5 (distal less homeobox5) stimulates osteoblast differentiation in mammals [20]. A number of *in vitro* studies have shown that dlx5 mediates BMP2-induced runx2 and osterix expressions [21,22]. In teleost, dlx5 is expressed during the developmental process of visceral skeleton [23] and medial fin fold [24] in zebrafish. Nevertheless, to the best of our knowledge, dlx5 expression in teleost scale has not been studied.

During scale regeneration, scale pocket-lining cells are capable of differentiating into scale-forming and scale-regenerating cells [25]. This significant osteoblastic potential is common to that of bone periosteum. The periosteum contains osteogenic cells in the cambial layer and fibroblasts in the fibrous layer [26–29]. Sire [30] observed that, when a scale is experimentally pulled off, the scale-forming cells are removed with the dermis, but the scale pocket-lining cells are not damaged. Furthermore, epidermal fragments remain at the posterior edge of each scale pocket. The restoration of the normal scale pattern in regenerated scales depends on the presence of the scale pocket-lining cells, and, if they are damaged, abnormal scalation patterns and abnormal scales are produced [31].

To elucidate osteoblastic actions during scale regeneration, we cloned eight osteoblast-specific genes, dlx5, runx2a, runx2b, osterix, RANKL, type I collagen, ALP, and osteocalcin cDNAs, from goldfish (*C. auratus*) ontogenic scale and analyzed their mRNA expression patterns in regenerating scales. This is the first report of the full coding sequence of osterix, ALP, and osteocalcin molecules in goldfish. In addition, we previously demonstrated that TRAP and cathK mRNA are expressed in multinucleated osteoclasts of goldfish scale [1]. In this study, we succeeded in cloning the nuclear factor of activated T-cells, cytoplasmic 1 (NFATc1), an early osteoclastic marker which has been previously reported in mammalian bone [32].

Furthermore, to study the factor that controls the onset of scale resorption and regeneration, we conducted intra-pocket autotransplantation of five groups of modified scales, *i.e.*, 1) methanol-fixed scale, 2) proteinase K-treated cell-free scale, 3) polarity reversal (upside-down) scale, 4) U-shape trimmed scale, and 5) circular-hole perforated scale. TRAP and ALP staining were performed to investigate scale resorption and scale regeneration. Additionally, in the present study, we analyzed osteoclastic and osteoblastic marker gene expression for the first two groups (methanol-fixed and proteinase K-treated transplants) and compared them with those in sham transplantations and ontogenic scales.

The ability of cementless joint replacement implants, dental implants, and rigid internal fracture fixation devices to restore function depends in part upon intramembranous bone regeneration [33]. Future advances in implant fixation and fracture repair may benefit from an improved understanding of intramembranous bone regeneration. Nevertheless, gene expression patterns during intramembranous bone regeneration are poorly understood. To date, a method such as mechanical ablation of the marrow cavity is a convenient model of intramembranous bone regeneration [34–38]. However, one of the weak points of this model is that it requires that the animal be sacrificed to observe tissue regeneration; thus, results from each regeneration stage cannot be obtained from the same animal. The results from our current study show that bone-related genes during scale regeneration show almost the same expression trends as those in bone marrow ablation-induced intramembranous bone regeneration [39–41]. Therefore, we consider goldfish scale as a possible new tool for studying the process of intramembranous bone regeneration.

Materials and methods

Animals

Goldfish (*C. auratus*) were purchased from a commercial source (Higashikawa Fish Farm, Yamatokoriyama, Japan) and kept under normal laboratory conditions before the start of experiments. All experimental procedures were conducted in accordance with Tokyo Medical and Dental University's Guideline for the Care and Use of Laboratory Animals.

Complementary DNA cloning

Ontogenic scales were collected from male goldfish (body length = 14.8 ± 2.7 cm) under anesthesia with MS-222 (Sigma). Total RNA was isolated from the collected scales by using ISOGEN (Nippon Gene) and kept at −80 °C until the start of experiments. RNA was reverse-transcribed to cDNA using SuperScript III (Invitrogen). The resulting cDNA was served as a template for touchdown PCR amplification using degenerate primers. Information on cDNA nucleotide sequences and mature protein amino acid sequences of dlx5, osterix, runx2a (MASNS and MRIPV isoforms [42]), runx2b (MASNS and MRIPV isoforms [42]), type I collagen, osteocalcin, and NFATc1 of teleosts was obtained from GenBank through the web pages of the National Center of Biotechnology Institution. PCR products of the length of interest were gel-purified and cloned into PCR2.1 vector (Invitrogen) and Ligation high (TOYOBO). The sequence analysis was performed by using a BigDye Terminator v3.1 Cycle Sequencing Kit (Applied Biosystems) and an automated DNA sequencer (ABI Prism 3100-Avant, Applied Biosystems).

Rapid amplification of cDNA ends (RACE)

We obtained 5′ and 3′ ends of osterix, ALP, and osteocalcin by RACE. Template cDNA was prepared by using a Super SMART PCR cDNA synthesis kit (Clontech). RACE was performed by using the adapter primer supplied in the cDNA synthesis kit and specific primers for cloned PCR fragment sequences.

Amino acid sequence analysis

Amino acid sequence alignments were performed with the Clustal W multiple sequence alignment program available on the website of the DNA Data Bank of Japan (DDBJ). The amino acid identity of each predicted polypeptide was compared with *Xenopus laevis*, *Mus musculus*, and *Homo sapiens*.

Analysis of osteoblastic marker mRNA expression in spontaneously regenerated scales

Scales on the left side of the body were removed from goldfish (N = 15) after anesthetization with MS-222. On days 7, 14, and 21, goldfish were anesthetized with MS-222 again, and both regenerating (left side) and remaining ontogenic (right side) scales were collected.

Total RNA was isolated from collected scales by using ISOGEN and treated with DNase I. Two micrograms of total RNA was reverse-transcribed at 50 °C for 60 min and 70 °C for 15 min in 40 μl of a mixture containing 2 μl of SuperScript III, 10 mM dNTPs, 2 μl of RNase inhibitor, and 20 μM oligo-(dT). Quantitative real-time PCR analysis of dlx5, runx2a, runx2b, osterix, RANKL, type I collagen, ALP, osteocalcin, and β-actin (GenBank ID: AB039726) was performed by using the SYBR® *Premix Ex Taq*™ (TaKaRa Bio Inc.) and Mx3000 P® QPCR System (Stratagene). Real-time PCR was carried out with 1 μg of the first-strand mixture in 10 μl of a PCR mixture containing 5 μl of SYBR® *Premix Ex Taq*™, 0.2 μl of the ROX reference dye, and 0.2 μl of each gene-specific primer (Table 1). The conditions for PCR amplification consisted of 10 s of initial denaturation at 95 °C followed by 40 cycles of denaturation at 95 °C for 30 s, annealing and extension at 65 °C for 30 s, and a single cycle for dissociation curve analysis (95 °C for 5 s, 55 °C for 30 s, and 95 °C for 5 s). To control for differences in starting mRNA conditions, the mRNA levels of β-actin were used as an internal standard. The relative values of target mRNA expression were calculated from the target threshold cycle values and β-actin threshold cycle values using standard curves.

Scale modification and autotransplantation

Ontogenic scales were removed from goldfish under anesthesia with MS-222 and divided into five equal groups for five different modifications, including 1) methanol fixation, 2) proteinase K treatment, 3) scale polarity reversal (upside-down), 4) U-shape trimming, and 5) circular-hole perforation. In the first group, scales were immersed in a 99.8% methanol solution for 5 min at room temperature.

Table 1
Primer sequences for quantitative real-time reverse-transcription PCR.

Primers	Nucleotide sequences (5′–3′)
Dlx5	
Dlx5-F	CCGAGCCCGAAGTGAGGAT
Dlx5-R	GAAGAGCTGGCGCTTTCCAG
Osterix	
Osterix-F	GACTGCCTGACCAGCGTCAA
Osterix-R	GAGGCACCAAGCCTCTCCAA
Runx2a[a]	
Runx2a-F	TCCCACTGGAGGTGCAACAA
Runx2a-R	GGGTGGTGGAGTGGATGGAG
Runx2b[a]	
Runx2b-F	GACAGCAGCAGCAGGACAGC
Runx2b-R	TGAGAAGGCAACACCGAGCA
RANKL	
RANKL-F	GCGCTTACCTGCGGAATCATATC
RANKL-R	AAGTGCAACAGAATCGCCACAC
Type I collagen	
Type I collagen-F	TGCAACCAGGATGCCATCAA
Type I collagen-R	ATGAGGCGCAGGAAGGTGAG
Alkaline phosphatase	
ALP-F	TGGACACAGCGGTGAGGAAA
ALP-R	GTGGGCATATGCTGCACTCG
Osteocalcin	
Osteocalcin-F	ATGCCTGAGCGCAGGTCTTC
Osteocalcin-R	CACAGGCCAGGTTTGCTTCA
NFATcI	
NFATc1-F	CTGTCGTGCGTTTTGGGAAAG
NFATc1-R	GATGCTGGTGTTTTGGCTGTAACC
Tartrate-resistant acid phosphatase	
TRAP-F	TGCTGGACACTGTGCTGCTG
TRAP-R	GGAACCTGGTTTCGGTGTCG
CathepsinK	
CathK-F	TGGGAGGGCTGGAAACTCAC
CathK-R	CATGAGCCGCATGAACCTTG
β-actin	
β-actin-F	CGAGCGTGGCTACAGCTTCA
β-actin-R	GCCCGTCAGGGAGCTCATAG

[a] Runx2a and runx2b primers were determined from the highly conserved area of MASNS and MRIPV isoforms.

In the second group, scales were immersed in a 0.05% proteinase K solution for 20 min. Using a microscope, we confirmed that this proteinase K-treated procedure caused the scales to become cell-free. Both groups were then repeatedly rinsed in distilled water and autotransplanted to their original scale pockets under anesthesia. In the third group, scales were upside-down autotransplanted immediately after being pulled off. In the fourth group, each scale was U-shape-trimmed at the rostral part using a 5 mm-diameter hole punch. In the fifth group, one circular hole was made at the central part of scale using a 1 mm-diameter hole punch. The goal of each modification was 1) methanol fixation was conducted to make all cells on the scales non-living cells; 2) Proteinase K treatment was conducted to make scales to be entirely cell-free by detaching all cells; 3) Scale polarity reversal (upside-down) was carried out to disrupt the correct cell-to-cell contact between the scale pocket and the scale cortex; and 4) U-shape trimming and circular-hole perforation were conducted to partially eliminate cell-to-cell communication between the scale pocket and the scale cortex. As a control, other scales were pulled out and immediately re-inserted in their original positions (sham autotransplant).

Histological observations of scale resorption and new scale formation

After autotransplantation, goldfish (N = 25) were anesthetized again, and transplanted scales were collected from each animal on days 3, 5, 10, and 15 for modified groups 1–3 (methanol-fixed scales, proteinase K-treated scales, and polarity reversal (upside-down) scales), and, on day 10, for modified groups 4–5 (U-shape trimmed scales and circular-hole perforated scales). These scales were immersed in 10% formaldehyde in a 0.05 M cacodylate buffer (pH 7.4) for 10 min at room temperature, rinsed in distilled water, and incubated at 37 °C in the dark for 1 h in a tartrate-resistant acid phosphatase (TRAP) staining solution [1,10,43]. An assay for TRAP consisted of naphthol AS-BI phosphate solution, diazotized fast garnet GBC base solution, sodium nitrite solution, acetate solution (pH 5.2), and 10 mM L(+)-tartrate solution. ALP staining was performed separately by using NBT/BCIP stock solution at 35 °C for 30 min [43]. After staining, they were observed under an optical microscope.

Measurements of osteoclastic and osteoblastic marker mRNA levels in methanol-fixed scales and proteinase K-treated scales at post-autotransplantation

Autotransplantation of methanol-fixed scales and proteinase K-treated cell-free scales was conducted in goldfish (N = 15) along with sham autotransplantations. On post-autotransplant day 3 and day 15, the autotransplanted scales and the remaining ontogenic scales were collected. Total RNA was isolated, and real-time RT-PCR analysis of NFATc1, TRAP, cathK, RANKL, dlx5, osterix, type I collagen, osteocalcin, and β-actin was performed as described above. Each gene-specific primer is shown in Table 1.

Statistical analysis

All results are expressed as the mean ± SEM. Statistical significance was assessed by one-way ANOVA followed by the Bonferroni method. The data of the relative expression amount of genes in autotransplanted scales at post-autotransplantation were analyzed after taking logarithms.

Results

Cloning of osteoblastic and osteoclastic marker cDNA from the scale of goldfish

RT-PCR amplification using degenerate primers was successfully employed to amplify the fragments of dlx5, runx2a (MASNS and MRIPV isoforms), runx2b (MASNS and MRIPV isoforms), osterix,

RANKL, type I collagen, ALP, osteocalcin, and NFATc1 shown in Table 2. Osterix, ALP, and osteocalcin fragments were subjected to 5′ and 3′ RACE, and then the sequence of the resulting 2064 bp, 2391 bp, and 469 bp cDNA was determined. The nucleotide sequence data of goldfish dlx5, runx2a (MASNS), runx2a (MRIPV), runx2b (MASNS), runx2b (MRIPV), osterix, RANKL, type I collagen, ALP, osteocalcin, and NFATc1 cDNA has been submitted to the DDBJ/EMBL/GenBank DNA database under each GenBank ID listed in Table 2. The comparison of the amino acid sequences of goldfish dlx5, runx2a (MASNS), runx2a (MRIPV), runx2b (MASNS), runx2b (MRIPV), osterix, RANKL, type I collagen, ALP, osteocalcin, and NFATc1 with *Danio rerio*, *X. laevis*, *M. musculus*, and *H. sapiens* is shown in Table 2. RANKL and osteocalcin have low degrees of identity with *X. laevis*, *M. musculus*, and *H. sapiens*. The other genes have greater than 80% homology with *D. rerio* and greater than 50% homology with other vertebrates. Concerning the full sequences, for osterix, residues of three zinc finger structures, a putative nuclear localization signal, and a repetitive motif, GSSPL, are conserved with the specific protein7 (Sp7)/osterix of humans and rodents [44], while the proline-rich domain shares low homology. For ALP, metal ligand sites and residues that interact with substrate phosphate [45] are conserved, whereas the N and C terminals have low homology to humans, rodents, and amphibians. For osteocalcin, the Gla region including the two Cys [46] and the teleost's unique highly conserved sequence near the C-terminal, AAYXAYYGP(I/P) [47], are highly conserved. Other regions of osteocalcin share low homology with tetrapods.

Expression pattern of osteoblastic markers in the spontaneous regenerating scale

We found that osteoblastic markers were expressed in the regenerating scale and that the expression of dlx5, osterix, type I collagen, ALP, and osteocalcin mRNAs increased remarkably during scale regeneration, although that of runx2a and runx2b mRNA was not higher than that of ontogenic scale (Figs. 1A–B). On day 7, Dlx5 mRNA expression reached the peak level and declined (Fig. 1C), whereas osterix mRNA expression increased and persisted (Fig. 1D). Two functional genes of osteoblasts, type I collagen and ALP, were expressed since the early stage of scale regeneration (Figs. 1E–F), while osteocalcin mRNA expression was increased later on day 14 (Fig. 1G).

Histological evidence of scale resorption and new scale formation

On day 5, transplantation in methanol-fixed and proteinase K-treated scales triggered apparent inflammation, bleeding, and edema in and around the transplant areas; the same was observed in polarity reversal (upside-down) scales, but with less inflammation. TRAP staining on day 5 indicated that osteoclastic activities in the methanol-fixed, the proteinase K-treated, and polarity reversal scales (Figs. 2A–C) were higher than those in the sham transplanted and ontogenic scales (Figs. 2D–E). Microscopically, the numbers of TRAP-positive cells were confirmed to be higher as well. The TRAP-positive area on scale increased with time (Table 3). On day 15, many multinucleated osteoclasts appeared (Fig. 3C), and the methanol-fixed and proteinase K-treated transplants were resorbed (Fig. 3B). Post-transplant new scale formation was found since day 10 on the posterior side of every modified transplanted scale, including methanol-fixed transplants (Fig. 2F), proteinase K-treated cell-free transplants (Fig. 2G), and the polarity reversal (upside-down) transplants (Fig. 2H). The new scales were positively stained with alkaline phosphatase. Each new scale began to adhere firmly to the posterior side of the transplant and grew larger on day 15. However, the shapes of these scales were not identical to those of spontaneously regenerating scales, and their sizes were smaller when compared with the same-age spontaneously regenerating scales. No new scale regenerated in the sham transplants (Fig. 2I). The sham transplants were well sustained in the scale pockets and were negative for TRAP and ALP staining on days 5 and 10 (Figs. 2D, I). In U-shape trimmed transplants (Figs. 4A–B) and circular-hole perforated transplants (Figs. 4C–F), new scales regenerated at the trimmed and perforated parts of each scale, respectively. In these two groups, scale resorption occurred apparently only around the trimmed/perforated part without obvious inflammation.

Osteoclastic and osteoblastic activities in post-autotransplant methanol-fixed scales and proteinase K-treated scales

At the early post-autotransplant stage (days 3), the mRNA expression amount of early osteoclastic marker NFATc1 in both groups of modified transplanted scales (methanol-fixed transplants and proteinase K-treated transplants) was significantly higher than that in

Table 2
Amplified fragment length and comparison of amino acid sequences of goldfish dlx5, runx2a (MASNS and MRIPV), runx2b (MASNS and MRIPV), osterix, RANKL, type I collagen, ALP, osteocalcin, and NFATc1 to *Danio rerio*, *Xenopus leavis*, *Mus musculus*, and *Homo sapiens*.

Amplified fragment	Length (bp)	Amino acid sequence homology (%)			
		Danio rerio UniProt ID:	*Xenopus laevis* UniProt ID:	*Mus musculus* UniProt ID:	*Homo sapiens* UniProt ID:
Dlx5	411 (partial)	96.06%	90.00%	80.71%	80.00%
GenBank ID: AB685218		Q5XJL9	Q6GLJ3	P70396	P56178
Runx2a (MASNS)	884 (partial)	95.28%	69.31%	61.65%	63.25%
GenBank ID: AB274884		Q6U1J2	A1YIX8	Q08775	Q5T802.
Runx2a (MRIPV)	1152 (partial)	95.41%	68.86%	71.37%	71.37%
GenBank ID: AB274885		Q596E7	A1YIX9	Q08775	Q5T802
Runx2b (MASNS)	678 (partial)	95.10%	72.17%	53.06%	56.43%
GenBank ID: AB274886		Q6TYZ4	A1YIX9	Q08775	Q5T802
Runx2b (MRIPV)	928 (partial)	97.84%	76.98%	86.36%	86.36%
GenBank ID: AB274887		Q4VW83	A1YIX9	Q08775	Q5T802
Osterix	2064 (full)	86.83%	50.86%	62.18%	64.56%
GenBank ID: AB274888		Q6U1J4	A6H8I6	Q2KHK9	Q8TDD2
RANKL	725 (partial)	–	32.89%	26.99%	26.38%
GenBank ID: AB459540		–	Q5HZR8	Q059M3	O14788
Type I collagen	399 (partial)	97.74%	85.71%	84.21%	82.71%
GenBank ID: AB685219		Q6P4U1	Q9IB91	Q99LL6	D3DTX7
ALP	2391 (full)	87.86%	76.08%	76.29%	77.11%
GenBank ID: AB459538		F1Q5B5	Q32NT2	Q8JZS4	B7Z4Y6
Osteocalcin	469 (full)	72.12%	29.13%	31.68%	28.71%
GenBank ID: AB685220		Q4G6A6	P40147	P86546	P02818
NFATc1	2544 (partial)	93.13%	62.38%	62.09%	61.80%
GenBank ID: AB685221		Q19AW4	Q6GNH6	Q6P7T9	B5B2M

Each accession number (UniProt ID) of the compared amino acid sequence is written one line below the percent homology.

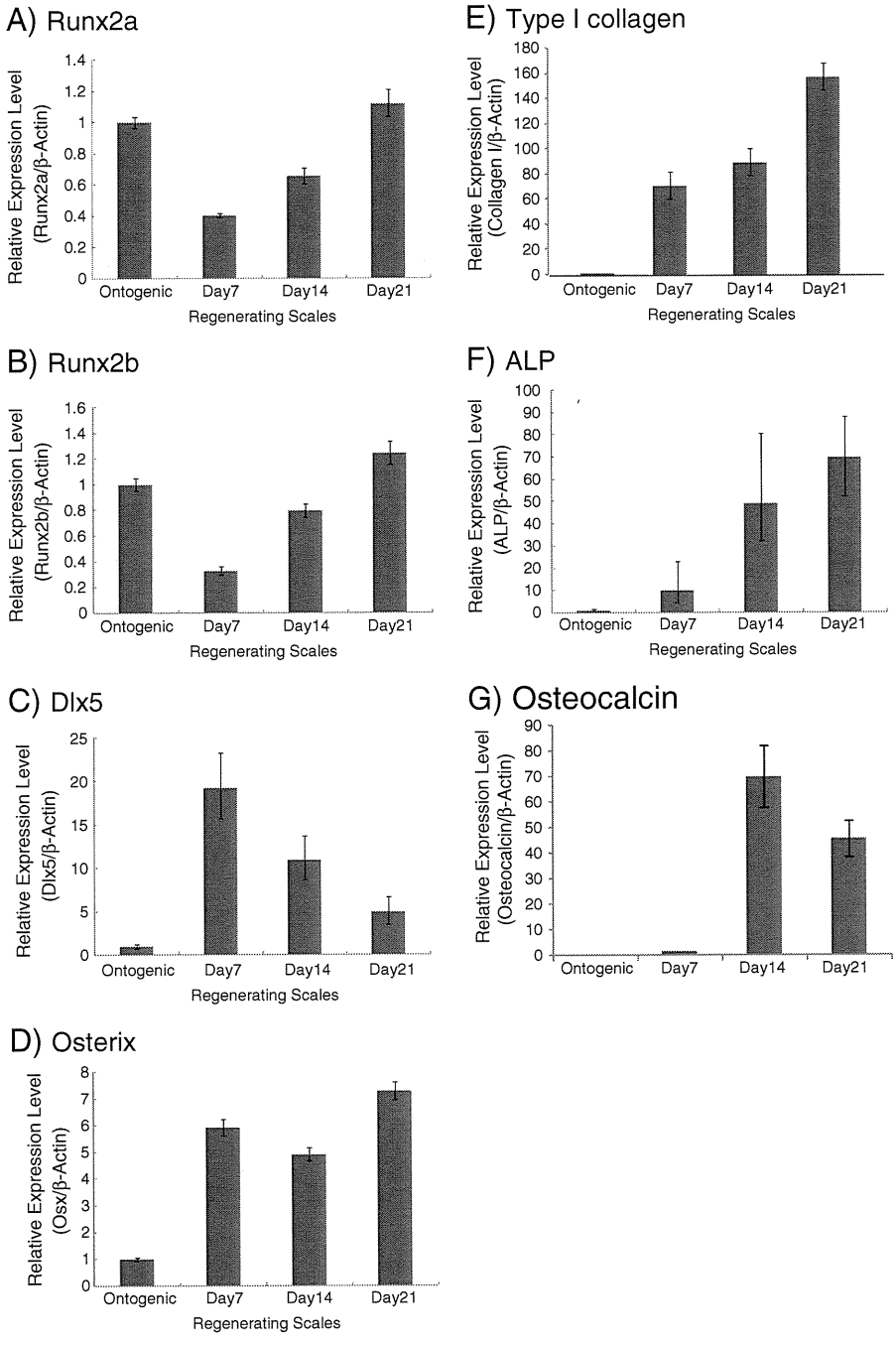

Fig. 1. (A–G). Expression patterns of osteoblastic markers during spontaneous scale regeneration compared to ontogenic scales. Column and bars represent the mean and SEM (N = 5), respectively.

the sham transplants and the ontogenic scales ($P<0.05$) (Fig. 5A), whereas no significant increase in expression of early osteoblastic marker dlx5, osterix (Figs. 5D–E), and runx2 (data not shown) was found. In addition, the methanol-fixed transplants and the proteinase K-treated transplant showed slightly higher, but insignificant, levels of cathK and RANKL (Figs. 5B–C). On the other hand, at the late post-autotransplant stage (days 15), two osteoclastic markers, TRAP and cathK, and two osteoblastic markers, collagen I and osteocalcin, in both methanol-fixed transplants and proteinase K-treated transplants were significantly higher when compared to sham autotransplants and ontogenic scales ($P<0.05$) (Figs. 6A–D). At this stage, no significant result was found in the mRNA expression analysis of NFATc1 (data not shown).

Discussion

For studying the bone metabolism, using goldfish scale is a simple, cost-effective, and time-saving approach. A goldfish has a total of more than one hundred scales on both sides of its body. Numerous scales can be pulled out at any time without fatal consequences. This condition enables *in vivo* experiments to investigate various stages of the osteo-regeneration process in real-time in the same animal. Moreover, from the same goldfish, harvested scales can be applied by several scale treatments/modifications *in vitro*. For example, scales are divided into several groups, and each groups is then treated differently depending on the experimental plan. This opens possibilities for more complex experimental designs. The effects of multiple environment factors can